

AD-A238 800



DAPS

①



CONSTRUCTION, CALIBRATION AND USE  
 OF A NEUTRON TIME-OF-FLIGHT  
 SPECTROMETER

THESIS

Charles C. Wood, LCDR, USAF

AFIT/GNE/ENP/81M-12

**DTIC**  
**SELECTE**  
**JUL 23 1991**  
**S D D**

**DISTRIBUTION STATEMENT A**  
 Approved for public release  
 Distribution Unlimited

\*Original contains color plates; All DTIC reproductions will be in black and white\*

DEPARTMENT OF THE AIR FORCE  
 AIR UNIVERSITY  
**AIR FORCE INSTITUTE OF TECHNOLOGY**

Wright-Patterson Air Force Base, Ohio

①

AFIT/GNE/ENP/91M-12

DTIC  
SELECTE  
JUL 23 1991  
S D D

CONSTRUCTION, CALIBRATION AND USE  
OF A NEUTRON TIME-OF-FLIGHT  
SPECTROMETER

THESIS

Charles L. Wood, LCDR, USN

AFIT/GNE/ENP/91M-12

Approved for public release; distribution unlimited

01 7 10 1 7

91-05747



AFIT/GNE/ENP/91M-12

CONSTRUCTION, CALIBRATION AND USE OF A  
NEUTRON TIME-OF-FLIGHT SPECTROMETER

THESIS

Presented to the Faculty of the School of Engineering  
of the Air Force Institute of Technology  
Air University  
In Partial Fulfillment of the  
Requirements for the Degree of  
Master of Science in Nuclear Engineering

Charles L. Wood, B.E.E  
Lieutenant Commander, USN

March 1991

Accession For	
NTIS CRARI	<input checked="" type="checkbox"/>
DTIC TAB	<input type="checkbox"/>
Unannounced	<input type="checkbox"/>
Justification	
By	
Distribution/	
Availability Codes	
Dist	Avail and/or Special
A-1	

Approved for public release; distribution unlimited

This report contains color  
plates; all DTIC reproductions  
will be in black and  
white.

## Preface

The purpose of this study was to construct, calibrate, and use a neutron time-of-flight spectrometer. The immediate need for this spectrometer was for use in the Nuclear Instrumentation Course currently being taught in the Graduate Nuclear Engineering (GNE) curriculum at the Air Force Institute of Technology (AFIT).

In performing the experimentation and writing this thesis I have received a great deal of help from others. I am deeply grateful to my thesis advisor, Dr. George John, Ph.D., for his knowledge of experimental procedures, patience when I was frustrated, and his knowledge of the English language and its use for relaying the information I have to others. I also would like to thank Mr. Bob Hendricks, lab technician, for his wit, patience, and assistance in understanding the vast resources available to me at the laboratory. LCDR Mathews is due a word of gratitude for his help with the understanding of the distribution functions and the Monte Carlo routine used. Finally, I would like to thank my wife, Karen, for her help in working out the final wording, punctuation, and organization of the paper, and for her understanding when I was short-tempered, with her and the kids, as the deadline neared.

## Table of Contents

	Page
Preface .....	ii
List of Figures .....	v
Abstract .....	vi
I. Introduction .....	1
Background .....	2
Scope .....	14
Assumptions .....	15
Sequence of Presentation .....	16
II. Experimental Considerations .....	17
Theory .....	19
Equipment .....	28
Circuit Operation .....	34
Procedure .....	38
III. Analysis and Results .....	48
Spectral Data .....	48
Average Energy .....	62
Error Analysis .....	63
IV. Discussion, Conclusions and Recommendations for Future Studies .....	71
Vita .....	75
References .....	76

Appendix A. Equipment list .....	A - 1
Appendix B. Timing and Calibration Procedures .....	B - 1
Appendix C. TK Solver Models Used for Analysis .....	C - 1

## List of Figures

Typical two detector TOF Spectrometer Geometry .....	12
Approximate Energy Ranges of Neutron Spectrometers .....	14
Experiment Geometry .....	18
Detector System .....	30
Experiment 3 Geometry .....	44
Proton Recoil Spectra from Detector 1 .....	47
Published Spectrum by Arun Kumar and P. S. Nagarajan ...	50
Time Spectrum for Experiment 1 .....	51
Energy Spectrum from Experiments 1 and 2 .....	53
Time Spectrum for Experiment 3 .....	54
Energy Spectrum for Experiment 3 .....	55
Experiment 6 Energy Spectrum .....	58
Comparison of published data with experimental data ....	60
Experiment 7 Dual Parameter Display .....	61
Error Analysis for High Energy Neutron Spectrum .....	68
Error Analysis for Mid-Range Neutron Energy .....	69
Error Analysis for Low Energy Neutron .....	70

**Abstract**

The energy spectrum of a 5 curie  $^{239}\text{Pu}$ -Be source is determined by constructing, calibrating and using a two detector neutron time-of-flight spectrometer. This spectrometer measures the time it takes for a neutron to travel from detector A to point B following an elastic scatter from a hydrogen atom. If the distance of travel is known, then the energy of the neutron is then calculated using kinematics. The different aspects of the construction, circuit operation, and experimental geometry are explained. The purpose of the construction of the spectrometer is for use in the Nuclear Instrumentation Lab at the Air Force Institute of Technology. The time spectrum obtained from the spectrometer is unfolded into the neutron energy spectrum. A comparison is made to the spectrum published by Arun Kumar and P. Nagarajan and others. The error analysis of the resolved energy spectrum is calculated using a Monte Carlo simulation routine which takes 1000 random points for the generation of the neutron in the source, and for the interactions in the sensitive volumes of both detectors. A dual parameter

analyzer is used to look at the coincidence response of the recoil protons from the first detector to the time spectrum from the experiment.

Construction, Calibration, and Use of a  
Neutron Time-of-Flight  
Spectrometer

1. Introduction

Since Chadwick first discovered the neutron in 1932, scientists and physicists have been trying to determine the energy spectra of different neutron sources. Several types of spectrometers have been developed through the years; however, only a few have an energy range wide enough to be practical. The time-of-flight system, which measures the time it takes for the neutron to travel from point A to point B, has emerged as the preferential choice for determining the energy spectrum. This system should provide the energy spectrum from any source, such as that emitted by spontaneous fission, by an ( $\alpha$ , n) reaction, or by any nuclear reaction. If the time for the travel of a fixed distance is known, then the kinetic

energy of the neutron can be calculated through kinematics. This report considers the different aspects of the construction of this type of spectrometer, the calibration and timing of the device, and its use to resolve the energy spectrum of a 5 curie  $^{239}\text{Pu}$ -Be neutron source.

### Background

The measurement of neutron energies with high resolution and somewhat reasonable efficiency is difficult for many reasons. The biggest factor contributing to this difficulty is the lack of a net electric charge on the neutron, which eliminates the use of all forms of electromagnetic and direct ionization spectrometers. Several methods have been developed over the years to measure the spectrum of different neutron sources. Among these are: (1) the measurement of proton recoil energies; (1:126) (2) the measurement of the energy release in a known nuclear reaction; (2:380) (3) diffraction of low-energy neutrons in crystals; (3:540) (4) time-of-flight measurements; (3:541) (5) threshold detectors; (4:708) and (6) measurement of attenuation and moderation of neutrons in various thickness of hydrogenous material, otherwise known as the use of Bonner Spheres.

(6:95) Each of these methods has advantages and disadvantages and each class is useful over different ranges of neutron energies.

At neutron energies above 100 keV, it is possible to detect neutrons with reasonable efficiency by detection of recoiling nuclei. Recoil protons, which are generated from hydrogenous material, are measured by both ionization and range measurements. If the proton recoil energies are measured irrespective of direction ( $4\pi$ ), then the spectrum of the protons must be "unfolded" by use of a computer program. However, if the proton recoil is measured only for the scatter of neutrons in a fixed direction relative to the direction of the incident neutron, then the neutron energy is directly calculable from the energy of the recoiling protons. The main disadvantage of this type spectrometer is associated with the detection of neutrons below 0.5 MeV. This limitation rises from the minimum track length for detection of proton recoil is about 3 microns. (3:540)

Soon after the discovery of the neutron, the low efficiency and difficulty in detecting neutrons with reasonable resolution resulted in the development of a number of spectrometers based on a neutron-induced reaction of the type  $n + A \rightarrow B + C + Q$ . For these reactions

the product particles are accompanied by an energy release,  $Q$ . This energy, along with the kinetic energy of the neutron, appears as the kinetic energy of the product particles, provided they are not in an excited state. Even though the individual energies of particles B and C will vary with their angles of emission, the total energy is always the sum of the energy,  $Q$ , and the kinetic energy of the incident neutron. The neutron energy is therefore obtained from a measurement of the total energy released.

For this type of spectrometer to be accurate, the reaction must satisfy several requirements. The cross section of the material, A, must be sufficiently large and a smooth function of the neutron energy. The products of the reaction must not vary in the decay of the excited atom which is generated when the neutron reacts with the nucleus. Additionally, if the low-energy range is to be considered, the value of the energy released,  $Q$ , must be positive and the material, A, must be of a form that is suitable for use in, or with, an energy sensitive detector. Currently, the only materials which come close to this are the light nuclei  $^3\text{He}$ ,  $^6\text{Li}$  and  $^{10}\text{B}$ .

The cross section for absorption of neutrons of  $^3\text{He}$  is about 5327 barns for 2200 m/sec neutrons and varies as  $1/v$  for neutrons up to approximately 6 MeV. (5:941) The

problem associated with this detector system is the competing reactions which reduce the number of (n,p) reactions. The most significant of these is the elastic scatter cross section for the nucleus of the helium atom. This scattering cross section is always higher than the absorption cross section, and it becomes more prominent at higher neutron energies. For example, the cross sections for absorption and scatter are about equal at a neutron energy of 150 keV, but the scattering cross section is about three times more probable than absorption at 2 MeV. Additionally, a competing (n,d) reaction on  $^3\text{He}$  is possible at neutron energies exceeding 4.3 MeV, but this cross section is low for neutron energies below 10 MeV. (4:527). Therefore, the upper limit on the energy of the neutrons which it can effectively detect is limited.

A widely used spectrometer for slow neutrons is the  $\text{BF}_3$  proportional tube system. This device uses boron trifluoride as the proportional-counter gas and  $^{10}\text{B}$  as the target for converting the slow neutrons into secondary particles. A number of other boron-containing gasses have been evaluated, but  $\text{BF}_3$  is the universal choice because of its superior properties as a proportional gas, as well as its high concentration of  $^{10}\text{B}$ . In most cases, the gas used for the proportional gas is highly enriched with  $^{10}\text{B}$ ,

so that the efficiency is some five times greater than if the gas contained naturally-occurring boron. This type detector gives a pulse height spectrum for the bombarding neutrons which is related to the energy spectrum of the neutrons.

A disadvantage arises with the use of the proportional-tube system because the output pulse from a  $\text{BF}_3$  tube originates with reaction products created with a random location and direction. This causes typical pulses with rise times that vary by as much as 3-5 microseconds for tubes of average size. (4:493) Another disadvantage is that the point of interaction cannot be precisely defined except as occurring somewhere in the volume of the gas. With a typical tube being 10-20 centimeters long to provide reasonable interaction efficiency, path-length uncertainties can be quite large. Therefore, this type of system is rejected for the application presented here.

Another widely used material for the detection of neutrons is  $^6\text{Li}$ . The neutron absorption cross section for a 2200 m/sec neutron is about 940 barns and varies as  $1/v$  for neutrons up to about 1 MeV with a pronounced resonance at 250 keV. (5:941) With this cross section, the use of  $^6\text{Li}$  becomes a very capable detector for low energies; however, for fast neutrons over 1 MeV the material becomes

ineffective. A competing reaction,  ${}^6\text{Li} (n,n'd) {}^4\text{He}$ , has a smaller Q value and becomes the dominant neutron-induced reaction above about 2.5 MeV. Because this reaction leads to three products, one of which is a neutron that normally escapes, a continuum of deposited energy should be expected even for mono-energetic incident neutrons. Therefore, even though it will contribute some neutron pulses, this additional reaction is generally an undesirable part of the response of any detector that attempts to measure the incident neutron energy. (4:524)

Crystal Diffraction neutron spectrometers with high resolution make use of the reflection of an intense well-collimated beam of neutrons at the Bragg angles associated with the atomic planes of a crystal. A highly collimated beam of neutrons from a nuclear reactor is allowed to fall on a large crystal at an angle  $\theta$  relative to the crystal planes. Some of the neutrons which have a wave length  $\lambda$  such that they satisfy the Bragg relationship are reflected through an exit collimator into a neutron detector placed at the angle  $\theta$  relative to the reflecting planes. This relationship for the detector is:

$$n\lambda = 2d\sin\theta \quad (1)$$

where  $n$  is an integer,  $\lambda$  is the DeBroglie wavelength of the neutron,  $d$  is the spacing between crystal planes and  $\theta$  is the angle between the direction of the incident neutron beam and the reflecting plane. The resolving power of this spectrometer is largely governed by the uncertainties in defining the angle  $\theta$ . Additionally, there is an intrinsic uncertainty introduced by imperfections in the crystal structure itself, and there is an ambiguity induced because  $n$  can have values of 1,2,3, etc. Thus if  $\lambda_2$  is equal to  $0.5\lambda_1$  and  $n_2 = 2$  and  $n_1 = 1$  then  $\theta_1 = \theta_2$  and the accuracy of the resolution is gone. Crystal spectrometers have been used, however, with great success up to energies of about 10 eV. Their performance deteriorates above this due to a loss in the counting rate as the neutron energy increases. (3:540-541)

None of the spectrometers mentioned thus far cover all energy ranges. There is, however, one type which will cover all energy ranges of interest, the time-of-flight spectrometer. Time-of-flight spectrometers measure the flight time between two fixed points. There are several different types of this spectrometer. The first of these is the pulse time-of-flight spectrometers, in which the neutrons are pulsed out of the source and the time it takes for the different energy neutrons to travel a fixed

distance,  $l$ , is measured. This time,  $\Delta t$ , is collected and the time spectrum converted into the energy spectrum of the neutron source. Not having a pulse accelerator at all facilities led into the development of a different type of time-of-flight spectrometer.

This type of spectrometer uses the scatter of a neutron from a hydrogenous material into a second detector a fixed distance away from the first detector. With this system, the time of the flight of a scattered neutron from the first detector to the second detector can be measured. Figure (1) is a typical set up for the two detector system. With the system configured this way the neutron could travel the distance from the source to the first detector, scatter into the solid angle of the second detector and generate both start and stop times for a device which could measure this flight time. The use of a time-to-amplitude converter does this job. By setting the time range of the converter to a maximum time in which the slowest neutron of interest (0.5 MeV) would take to traverse the distance between the detectors signals of different pulse heights would be generated for the various flight times. These signals could be fed into a Multi-Channel Analyzer and the time spectrum generated over a period of time. Care must be taken when the time

spectrum is unfolded into the energy spectrum of the neutron source in order to properly calculate the incident neutron energy. For scattered neutrons which are not relativistic, this time-of-flight,  $\Delta t$ , is given in nanoseconds by the relation

$$\Delta t = \frac{72.3l}{E^{1/2}} \quad (2)$$

where  $l$  is the length of the flight path in meters and  $E$  is the energy of the neutron in MeV. By determining the values of  $\Delta t$  over a fixed distance  $l$ , the energy spectrum for any neutron source can be determined. Should the neutrons approach the rest mass of the neutron (939.566 MeV), equation 2 is no longer valid and the kinetic energy of the neutron,  $E_n$ , can be determined through the use of the familiar result of special relativity: (1:541)

$$E_n = E_0 \left[ \left( 1 - \frac{v_n^2}{c^2} \right)^{-\frac{1}{2}} - 1 \right] \quad (3)$$

where  $E_0$  is the rest mass of the neutron and  $c$  is the speed of light. Substituting  $v = l/\Delta t$  yields

$$E_n = E_0 \left[ \left( 1 - \frac{l^2}{\Delta t^2 c^2} \right)^{-\frac{1}{2}} - 1 \right] \quad (4)$$

If the units of energy are MeV, and those of length and time are meters and nanoseconds, respectively, then the time it takes in nanoseconds for the neutron to travel distance  $l$ , is

$$\Delta t = \frac{3.3356410l}{\left[ 1 - \left( \frac{E_0}{E_n + E_0} \right)^2 \right]^{\frac{1}{2}}} \quad (5)$$

Since the time of travel can be measured with a proper geometry set-up of equipment and the proper electronics, the energy of the scattered neutron  $E_n$  can be calculated. Therefore, the energy limitations which existed on the other types of spectrometers do not exist with the time-of-flight system which is its biggest advantage. Another advantage of the time-of-flight system is the simplicity of the electronics involved. The use of a time-to-amplitude converter to measure the flight time is

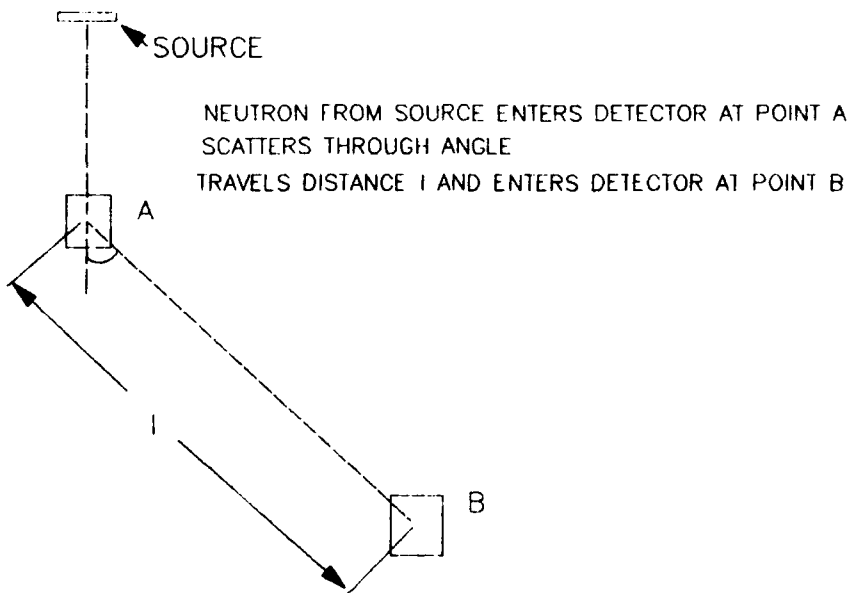


Figure 1. Typical Two Detector  
Time-of-Flight Spectrometer Geometry

vital to the ease in which the time spectrum can be generated for the two detector system. The greatest disadvantage of the system is its inefficiency. This inefficiency comes about, for small neutron sources, from the number of scattered neutrons which are incident on the second detector, resulting in long counting times in which the linearity of the counting system may fail.

The primary concern for the measurement of neutron spectra is the energy range that the method will cover.

Figure (2) is a graphical representation of the energy ranges that can be effectively analyzed by the different detection methods. (6:96)

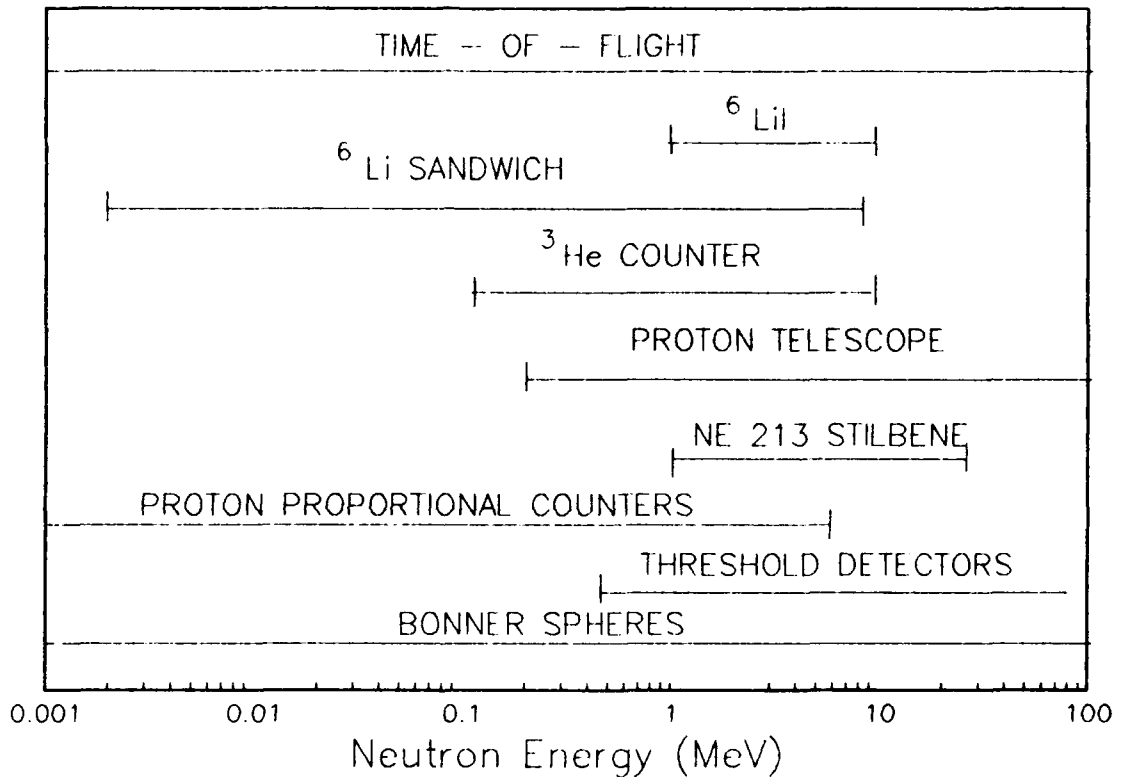


Figure 2. Energy Ranges for Neutron Spectrometers

As depicted in figure (2), the best overall energy spread is obtained with either a time-of-flight spectrometer or with a Bonner sphere system. The

limitations of the energy range of the other detectors does not lend itself to this study of the energy spectrum from a neutron source such as  $^{239}\text{Pu-Be}$ , which is the source of neutrons for analysis in this report.

### **Scope**

The scope of this project deals with the different aspects of the time-of-flight spectrometer setup, calibration, and use. The main objective of this study is to construct, test, calibrate and use a neutron time of flight detector. This is accomplished through the use of experimentation along with the unfolding of the time spectrum into the energy of the incident neutrons. A 5 curie  $^{239}\text{Pu-Be}$  source will be used to test the detectors and prove out the electronics. The energy range of this source is from 0.5 MeV to 10.5 MeV. Therefore classical kinematics will be used for the resolution of the energy spectrum from the time spectrum.

### **Assumptions**

In order to complete the study, the following assumptions are made:

(1) The response of all electronic equipment is linear.

(2) During the time-of-flight measurement, the fast neutrons will not overtake slow neutrons causing errors to be generated in the time spectrum.

(4) All measurements of length in the lab will be accurate to  $\pm 2\%$ .

(5) Multiple scatters in the sensitive volumes of the detectors can be neglected which would degrade the energy of the incident neutron yielding a softer energy spectrum.

(6) The neutrons will travel in a straight path between the two detectors.

(7) Even though the plastic scintillators have almost as many carbon atoms as hydrogen atoms, the scattering of the neutrons from these atoms will not be considered.

### Sequence of Presentation

The theory of the unfolding of the time spectrum into the energy spectrum of the incident neutrons is discussed, along with the factors that deal with the detection efficiency. Following this, the equipment selected for the detection system is described along with the operation of those items which may not be familiar. The procedure

for the experimentation is explained in detail and the results, along with the error analysis, provided. Finally, the conclusions are reached concerning the detection system and the analysis of the data.

## II. Experimental Considerations

To successfully undertake this assignment a spectrometer is constructed to process the signals from the anodes of two plastic scintillator detectors which correspond to the time difference between a start signal and a stop signal generated by the same neutron. Constant fraction discriminators, (CFD), are used to reduce the signal jitter from the anodes and to eliminate the dependence of the amplitude of the signal. The start and stop signals are fed into a time-to-amplitude converter which will generate a 0 to 10 volt logic signal, depending on the time between start and stop signals and the time range selected for analysis. A time spectrum is generated and this spectrum unfolded to produce the energy spectrum of the source. This system is set up initially in a high scatter environment with the use of a neutron moderator to form a collimated beam of neutrons from the source. The geometry of the detector set up for experiments 1 and 2 is shown in figure (3). Experiment 1 will have the detectors 1.5 meters apart and experiment 2 will place the detectors 0.65 meters apart.

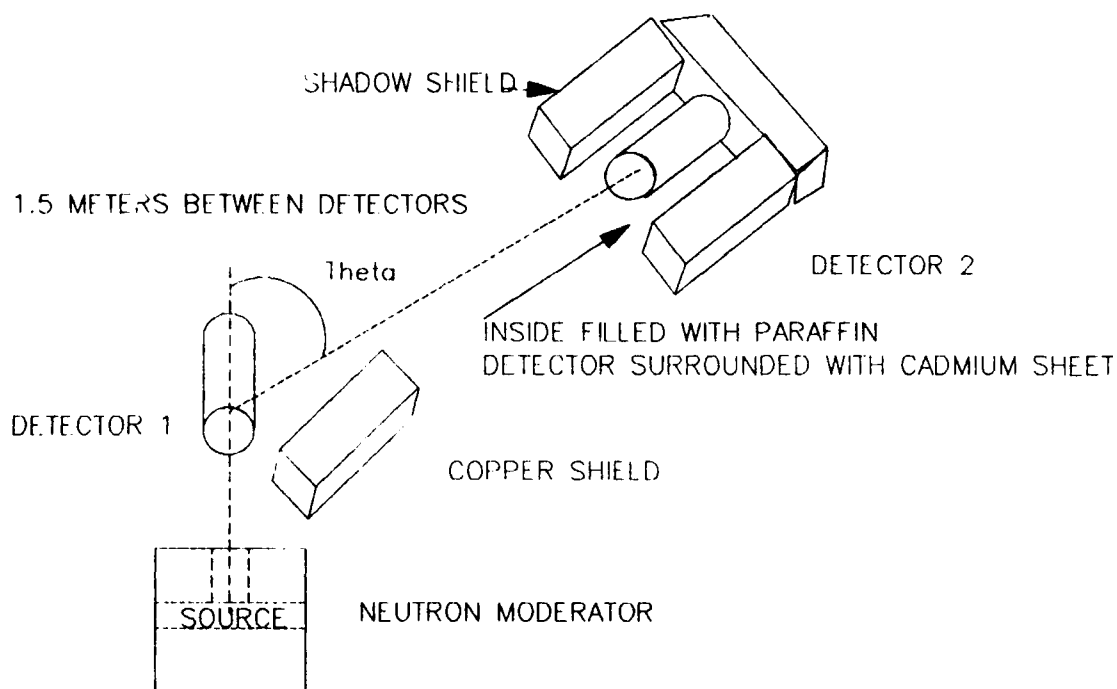


Figure 3. Experiment Geometry

The copper shield reduces the number of first flight incident neutrons from the source on the second detector. The shadow shield helps attenuate the number of second and third scatter neutrons from the surroundings of the detectors. A discussion on the construction of the shadow

shield is given in a later section of the document. Following the experiments within the high scatter environment, the detectors and electronics are moved into a low scatter environment and the experiments rerun. After a detailed analysis of the data obtained from the first four experiments, the plastic scintillators are replaced with ones that have twice the volume of the first ones and the experiments conducted again. With this complete, an analysis is done using the dual parameter feature of the analyzer, by placing the recoil proton spectra on one axis, the time-of-flight information on the other axis, and determining the relationship between the proton recoil energy and the time-of-flight information.

### Theory

The detection of high energy neutrons has challenged scientists and physicists since the early 1930's. The most common method of determining the presence of these neutrons is based on the scattering of the neutrons by light nuclei. Elastic scattering transfers some portion of the energy into the target nucleus, which recoils and acts much like a proton or alpha particle as it loses its energy in the detector medium. Because of its relative

size to that of the neutron and its behavior as a recoil proton, hydrogen is the preferred choice. To maximize the number of hydrogen molecules per cubic centimeter, plastic scintillators were selected to generate the recoil proton and subsequent signals from the interaction of the neutrons.

To begin the signal generation in the sensitive volume of the scintillators, the target nuclei are for all practical purposes at rest prior to the collision. During a single hydrogen collision, the amount of energy transfer to the nucleus can be from 0 to the full energy of the neutron, which results in a signal proportional to the energy deposited. To examine this better, the kinematics of neutron elastic scattering must be investigated.

A center of mass system with non-relativistic neutrons ( $E_n \ll 939 \text{ MeV}$ ) is assumed. By conserving momentum and energy we are able to determine the energy of the scattered neutron from the inelastic collision with a proton by use of the equation

$$E_s = \frac{2A}{(1+A)^2} (1 - \cos\Theta) E_N \quad (6)$$

where  $A$  is the mass of the target nucleus,  $E_n$  is the energy of the incoming neutron,  $E_s$  is the energy of the scattered neutron, and  $\theta$  is the scattering angle of the neutron in the center of mass system.

To convert this equation into a laboratory system where the protons are initially at rest, we use the transformation

$$\cos\theta = \sqrt{\frac{1 - \cos\Theta}{2}} \quad (7)$$

where  $\theta$  is the scattering angle of the recoil nucleus.

Combining the last two equations we have

$$E_s = \frac{4A}{(1+A)^2} (\cos^2\theta) E_n \quad (8)$$

which for neutrons which scatter from hydrogen atoms reduces to

$$E_s = (\cos^2 \theta) E_n \quad (9)$$

Scatters of neutrons from carbon atoms, within the sensitive volume of the detector, will impart only 14% of their energy into the scintillator which will make the energy spectrum below 1.5 MeV suspect to the final resolution. This results from calculation of equation (8) using the value of 12 for the atomic number of carbon and assuming a scatter angle of  $45^\circ$ . Therefore, the assumption that the carbon atoms will not contribute to the final resolution is somewhat valid.

To determine the value of  $E_s$ , classical kinematics along with the application of distribution function manipulation is used. To do this we start with the equation of kinetic energy for the neutron

$$E_s = \frac{1}{2} m v^2 \quad (10)$$

If the neutron travels from the first detector to the second detector a known distance  $l$  in time  $\Delta t$ , then the velocity of the neutron is

$$v = \frac{l}{\Delta t} \quad (11)$$

By differentiating the equation with respect to  $\Delta t$  we get

$$\frac{dv}{d(\Delta t)} = -\frac{l}{\Delta t^2} \quad (12)$$

or that  $dv = -l/\Delta t^2 dt$ . To eliminate dependence on the number of particles the spectrum of the time, velocity, and energy will be reduced to a normalized spectrum. To accomplish this, the time spectrum, which is measured in the laboratory, is divided by the total integral of the spectrum resulting in  $S(\Delta t)$ . This relationship is needed

for the next step in the derivation, which is to go from the time distribution to the velocity distribution and finally to the energy distribution through the use of

$$S(v) = S(\Delta t) \frac{d(\Delta t)}{dv} \quad (13)$$

which leads to

$$S(v) = S(\Delta t) \frac{\Delta t^2}{l} \quad (14)$$

Correlating the energy to the velocity gives

$$S(E_s) = S(v) \frac{dv}{dE_s} \quad (15)$$

Returning to equation (9) we find the alliance between the energy of the particle to the velocity  $dE_s/dv$  of the particle to be

$$\frac{dE_s}{dv} = mv \quad (16)$$

and

$$\frac{dv}{dE_s} = \frac{1}{\frac{dE_s}{dv}} = \frac{1}{mv} = \frac{\Delta t}{ml} \quad (17)$$

substituting the previous values for  $v$ ,  $dv$ , and realizing that the value of  $dv$  is the absolute value of the relationship in equation (12), we have

$$\begin{aligned} S(E_s) &= S(v) \frac{dv}{dE_s} \\ S(v) &= S(\Delta t) \frac{d(\Delta t)}{dv} \\ S(E_s) &= S(\Delta t) \frac{d\Delta t}{dv} \frac{dv}{dE_s} \\ S(E_s) &= \frac{S(\Delta t)}{\frac{dv}{d\Delta t} \frac{dE_s}{dv}} = \frac{S(\Delta t)}{\left(\frac{l}{\Delta t^2}\right) m \left(\frac{l}{\Delta t}\right)} \end{aligned} \quad (18)$$

$$S(E_s) = \frac{\Delta t^3}{ml^2} S(\Delta t) \quad (19)$$

or that the distribution of particles of the scattered energy is equal to the constants in equation (19) times the value of the distribution in time  $t$ . The energy of the source neutron is found by normalizing the energy spectrum from the relationship in equation (9).

$$S(E_S) = S(E_N) \text{Cos}^2 \theta \quad (20)$$

which converts to the total transformation of the time spectrum into the incident neutron energy spectrum by using

$$S(E_N) = S(\Delta t) \frac{\Delta t^3}{m l^2 \text{Cos}^2 \theta} \quad (21)$$

The intrinsic detection efficiency of any detector based on recoil nuclei can be calculated from the scattering cross section  $\sigma_s$ . For the Bicron scintillators we have both carbon and hydrogen atoms, and the competing effects of the carbon scattering must be taken into account. Utilizing the relationship in Equation (8), for the carbon atoms with an atomic number of 12, and a scatter angle of  $45^\circ$ , results in a transfer of 14 % of the energy of the incident particle into the carbon atom. To ensure the data from the recoil of the

neutron from the hydrogen atoms is not contaminated, the Lower Level Discriminator, (LLD), must be set to eliminate the carbon scatters. The intrinsic efficiency for an axial beam of neutrons, neglecting multiple scatters within the sensitive volume of the detector, is given by

$$\epsilon = \frac{N_H \sigma_H}{N_H \sigma_H + N_C \sigma_C} (1 - \exp(-(N_H \sigma_H + N_C \sigma_C)d)) \quad (22)$$

where the subscripts H and C refer to the separate hydrogen and carbon quantities, and d is the path length of the neutron travel. (5:534)

Equation (22) can be explained in the following manner. The first term of the equation is the probability of the incident neutron coming in contact with a hydrogen atom vice the carbon atom. The second term is the probability that a neutron which travels a distance, d , in the sensitive volume medium will have an interaction with the medium. Therefore, the probability of interaction with a hydrogen atom times the probability of interaction within the medium converts to the intrinsic efficiency for the detector.

An empirical fit to the hydrogen scattering cross section given by Marion and Young is

$$\sigma_s(E_n) = \frac{4.83}{\sqrt{E_n}} - 0.578 \text{ barns} \quad (23)$$

where the energy of the incident neutron  $E_n$  is in MeV (5:521). The cross section for the carbon atoms in the region of interest has many resonance peaks in the area of the energy spectrum and would have to be individually calculated. For this study the average cross section of the carbon atoms is placed at 2 barns. With this cross section, the probability of entering into a collision with the carbon atoms is greater than for the hydrogen atoms. This leads to a lower intrinsic efficiency of the system and a source of possible erroneous signal generation in the detectors. Most of this is overcome by the adjustment of the Lower Level Discriminator. The efficiencies of the detectors will be calculated and reported in the results section of this report.

## Equipment

The detectors and electronics used for the detection system were selected based on the response characteristics of the different modules. A detailed list of equipment used in the detection system is listed in Appendix A. The detection circuit is shown in figure 3.

Several factors went into the selection of the different components. The desirable features of a neutron detector used in a time-of-flight spectrometer are:

(3:559)

- 1) high efficiency which is a slowly varying function of energy,
- 2) low efficiency for detecting background radiation,
- 3) fast time response, preferably in the nanosecond range,
- 4) ease of manufacture in various shapes and sizes,
- 5) simplicity of the associated electronics.

Based on these features, the use of an organic scintillator was selected for the detectors. The first scintillator used was a Bicron 422 plastic scintillator which is made of Polyvinyltoluene and has a decay time of

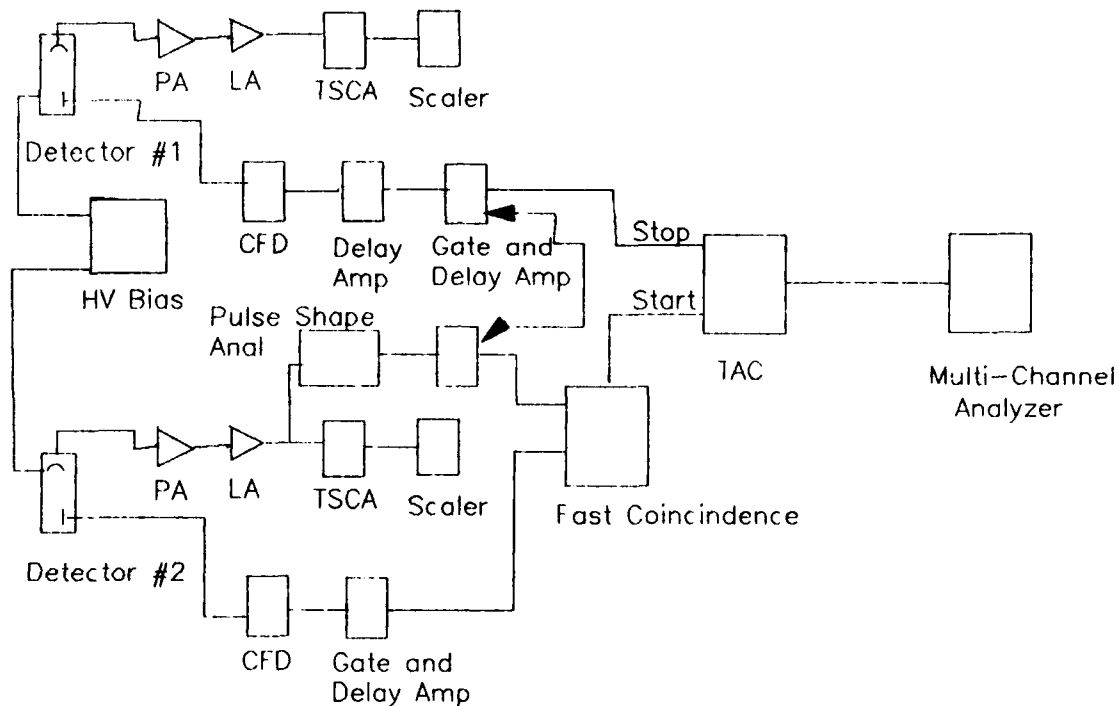


Figure 4. Detector System

Abbreviations used in figure (3) include: PA = Preamp,  
 LA = Linear Amp, CFD = Constant Fraction Discriminators,  
 TSCA = Timing Single Channel Analyzer, TAC =  
 Time-to-Amplitude Converter.

1.6 nanoseconds. The scintillator was a cylinder 2 inches in diameter and 1 inch high and had a carbon to hydrogen molecular ratio of 0.91. This scintillator was used for experiments 1-4. Following experiment 4 the scintillators in both detectors were exchanged for a Bicron 404 plastic scintillator coated with a titanium dioxide on the outside of the cylinder with the two flat faces clear. This scintillator is also made of Polyvinyltoluene, has a decay time of 1.8 nanoseconds, and is the same diameter as the previous ones except the height of the scintillators is 2 inches and has a carbon to hydrogen molecular ratio of 0.91 also. This doubled the volume of the scintillators, and with the hydrogen concentration of the two scintillators nearly the same ( $5.21 \times 10^{22}$  atoms/cm<sup>3</sup> vs  $5.19 \times 10^{22}$  atoms/cm<sup>3</sup>), the number of neutron interactions were expected to double on the first detector and increase by a factor of four on the second detector. The signals generated from the scintillators will vary in size depending of the amount of energy deposited and the angle of scatter from the first and second detectors. A timing device was used to reduce this dependence.

Because the base routes negative high voltage to the photo-cathode of the photo-multiplier tubes and the anode is grounded, the detector assembly consisting of the

scintillator, photo-multiplier tube and base had to be modified. To prevent a voltage drop across the glass envelope of the photo-multiplier tube and to minimize accidental shock, aluminum foil was used to cover the scintillator and a portion of the tube. A wire was soldered from the high voltage input at the bottom of the base and attached to the aluminum foil with black electrical tape. This modification kept the photo-cathode and the scintillator at the same negative potential. To minimize loading of the power supply in case of a short, a 10 M $\Omega$  resistor was added in series between the high voltage input and the aluminum foil.

Black electrical tape was utilized to prevent the scintillators from coming off and to prevent light leaks which could render the photo-tubes useless. Furthermore, an aluminum cover and end cap were slipped over the tube assembly and grounded to the base structure by screws to protect the user.

Constant fraction discriminators were used to reduce the jitter of the output of the anodes and to eliminate the amplitude dependence on the output of the signal. This technique is particularly useful with detectors in which the collection time varies according to the location of the initial ionization in the detector. The constant

fraction technique operates as follows: An incoming unipolar signal is split into two paths. The signal is attenuated in one path, and in the other path the signal is not attenuated, but delayed. The attenuated and delayed signals are then combined in a differential amplifier stage, resulting in a subtraction process. This signal is bipolar, with the baseline crossing being the locus of a particular point on the leading-edge of the incoming signal. This point is at a fraction of the amplitude of the incoming signal, and that fraction does not vary with amplitude. A crossover pickoff circuit generates a negative logic pulse which is time correlated to the desired leading edge fraction. These devices generate the timing signals for the time-to-amplitude converter.

A time-to-amplitude converter was selected based on its time scales and time resolution. Input signals are generated by the detection system to give a start and stop signal for the device. Based on the time between start and stop signals, the range selected, and the multiplier setting, a logic signal from 0 to 10 volts is generated. The Tennelec model selected has a range selection of 25 nanoseconds to 3 milliseconds. For a neutron source with an energy range of 0.5 to 10.5 MeV, these limitations

place a spread in the distance between the two detectors such that  $0.6 \leq l \leq 95.074$  meters. With this large of a spread in the values of  $l$ , the two detectors can be placed in an infinite number of positions. However; the further apart the detectors are, the less efficient the system becomes. The longer flight paths lead to a fewer number of neutrons which are incident on the second detector through spherical divergence, however; the longer flight paths gives a better definition of the scatter angle  $\theta$ . To optimize the trade-offs and to improve the efficiency of the spectrometer, the maximum distance for consideration was placed at 1.5 meters. Time resolution of the converter is listed as 0.01% of full scale plus 5 picoseconds.

### Circuit Operation

To generate a time spectrum, the electronics of the system must be able to select those neutrons which are incident on the first detector and then scatter into the second detector and interact. Should the electronics be able to do this, then the time spectrum can be generated through the use of a time-to-pulse-height converter (TTPHC).

Start and stop signals for the time-to-amplitude converter must be generated to obtain a time spectrum. To obtain these signals, a neutron from the source traverses the air, enters the sensitive volume of the first detector, has an elastic collision with the first detector and the recoil proton generates a negative signal on the anode in the first detector. If the same neutron scatters in the direction of the second detector and has an elastic collision with the hydrogen molecule in the sensitive volume, it will generate a signal at the anode of the second photo-multiplier. Because of the many orders of magnitude of neutrons which are incident on the first detector and scatter in many different angles, the signals from the first detector do not always result in a signal generation in the second detector, which could overwork the TTPHC. To eliminate overworking the TTPHC, the signal from the first detector is delayed through the use of a fixed time delay which allows the time-to-amplitude converter to look only for response pulses from the neutrons which make it to the second, or scattered detector. The delay time must be greater than the amount of time it would take for the slowest neutron to travel the distance between

the two detectors. These signals from the photo-tube anodes are fed to the constant fraction discriminators which generate a negative logic pulse. From the fixed delay, the signal from the first detector is sent to a gate and delay circuit to correct for differences in the signal generation timing caused by the electronics and then to the stop side of the time to amplitude converter. The signal from the second detector constant fraction discriminator is also sent to a gate and delay circuit for timing purposes, and then to a fast coincidence circuit awaiting the response of the Pulse Shape analyzer.

Since to the differential cross section of the hydrogen atoms is nearly constant for scattering into any angle  $\theta$ , the neutrons scatter isotropically from the first detector, of which a certain percentage are incident on the second detector. The percentage of scattered neutrons that are incident on the second detector depends principally on the distance between the first detector and the second detector. For those neutrons which interact with the second detector, a pulse similar to that from the first detector is generated. To prevent any direct flight neutrons from contaminating the data, a copper bar, with

measurements of 3" X 4" X 24", was placed between the second detector and the source (See figure 2). The copper bar allows the neutron to scatter, lose energy and become absorbed through an (n, $\gamma$ ) reaction. These photons could interact with the sensitive volume principally through Compton scatter to produce a signal which would effect the neutron data.

Interference from these photons is eliminated by using a Pulse-Shape-Analyzer. This device filters out all signals which have a fall time of less than 1 microsecond from the dynode of the second detector. The photons produces signals that have fall times less than this and the neutrons produce signals that are greater than this value. Timing for the fast coincidence circuit is provided for the output signal of the Pulse Shape Analyzer through a gate and delay timing module. A signal which makes it through the Pulse Shape Analyzer is from a neutron, not a photon, and this signal, when in coincidence with the anode signal, will generate the start signal for the time-to-amplitude converter. Therefore, the second detector generates the start signal after pulse shape analysis and the first detector generates the stop signal.

To generate proportional pulse heights corresponding to the different time-of-flights, the time-to-amplitude converter time range is set equal to the delay time of the fixed delay amp in the first detector. Measurements of TOF were made for separation distances between the two detectors. Since a lower bound of 0.5 MeV was selected for the range of energies to be measured, the longest flight times for the neutrons to travel 1.5 and 0.65 meters are respectively 153 nanoseconds and 100 nanoseconds. Therefore, the signals from the first detector was delayed by 200 nanoseconds to allow the signal from the second detector to start the TTPHC.

To generate only an 8 volt signal for the multi-channel analyzer, the multiplication potentiometer was set at 1.25. This ensured that the maximum voltage for a 200 nanosecond travel would be 8 volts.

### **Procedure**

A total of seven experiments were conducted to study various response of the neutron spectrometer. In the first two experiments time-of-flight spectrum were

measured in a high-scatter environment, and with the use of the neutron moderator to form a collimated beam of neutrons. This environment consisted of concrete floor along with concrete block walls to scatter the neutrons. Detectors were set up as illustrated in figure 2, and the detector circuit connected as depicted in figure 3. A negative high voltage of -2200 volts was placed on the photo-tubes and allowed to stabilize for twenty-four hours. The detection system was timed and calibrated using the procedure described in Appendix B.

The source selected for analysis is a  $^{239}\text{Pu}$ -Be source obtained from the Monsanto Research Corporation in Miamisburg, Ohio in 1962. The initial activity strength of the  $^{239}\text{Pu}$  was 5 curies with a total output of  $9.04 \times 10^6$  neutrons per second when first purchased. However, because the source is contaminated with a small amount of  $^{241}\text{Pu}$ , the number of neutrons emitted has increased. Today the number of neutrons that the source produces is  $1.1 \times 10^7$  per second. This increase is caused by the decay of  $^{241}\text{Pu}$  to  $^{241}\text{Am}$  which then decays by the emission of an  $\alpha$  particle. With the increased number of  $\alpha$  particles to react with the Beryllium, the number of neutrons increases.

Emission of neutrons from the neutron source is anisotropic because of its shape and cladding. The  $^{239}\text{Pu-Be}$  source is a cylinder 9.45 centimeters long and 2.08 centimeters in diameter enclosed with Tantalum and stainless steel. Thus, more neutrons will exit at  $90^\circ$  to the cylindrical axis than axially through the ends. The anisotropy factors relative to isotropic emission for the source, M1170, are cited as 1.071 at  $90^\circ$  to the axis and 0.48 at the ends.

A four-mil cadmium sheet was placed in the path of the neutrons to eliminate the thermal neutron contribution to the time-of-flight spectrum. Cadmium has an absorption cross section for thermal neutrons of about 19,910 barns, and can effectively absorb all neutrons below 0.5 eV.

The first experiments were set-up using the geometry in figure (3). When the experiment was first attempted, the data did not respond as predicted. The low energy end of the spectrum was very high and the upper end was low. Investigation into this revealed that the second detector was receiving over a factor of ten times the expected number of counts. To reduce this number and bring the counts down on the second detector, the shadow shield was built.

Material for the shadow shield consisted of reactor grade graphite and paraffin, which contains a large amount of hydrogen atoms. To compute the thickness of graphite necessary for the moderation of the most energetic neutron, the macroscopic cross section for the atoms was needed. This property for graphite is given in Table 1-4 of *Nuclear Reactor Theory* by LaMarsh as  $0.3851 \text{ cm}^{-1}$  which equates to a mean free path for the neutron to be 2.59 cm. A neutron of 11 MeV which maintained 71.6% of its energy following a collision with a carbon atom, would require a total of 10 collisions to reduce its energy down to less than 0.5 MeV (7:168). Therefore, a total of 25.9 centimeters or 10.2 inches of graphite were needed to moderate the neutrons scattered from the walls and floor. The paraffin was added to ensure the moderation of the neutrons prior to striking the detector. The detector was covered with a 4-mil sheet of cadmium to prevent these thermalized neutrons from entering the detector. The paraffin and carbon were not placed in front of the sensitive volume of the detector to allow the scattered neutrons from the first detector to enter the sensitive volume without moderation. With the shield in place, the number of counts on the second detector reduced by a factor of seven over that of an unshielded detector.

The first experiment continued for 104 hours before the time spectrum evolved into a useful piece of data. The different sections of the spectrum were smoothed by using a feature on the dual parameter analyzer known as the smooth command. This feature statistically smooths irregularities in spectra without altering the sizes and shapes of the spectral peaks. It performs a 5-point data smoothing of the spectrum in a region of interest. Smoothed data (S) are calculated from spectral data (Y) in channel n by the equation

$$S(n) = \frac{17Y(n) + 12(Y(n-1) + Y(n+1)) - 3(Y(n-2) + Y(n+2))}{35} \quad (24)$$

Smoothed data allow for a smoother energy spectrum from the unfolding of the time spectrum.

In the second measurement, the second detector was placed 65 centimeters from the first detector and the delay time in the anode circuit of the first detector changed to 100 nanoseconds. The calibration and timing were repeated using the procedure described in Appendix B. Experiment 2 produced a usable spectrum in one day;

however, the data was allowed to accumulate over the same time interval as experiment 1 to check the number of data points collected for the same time interval.

Experiments 3-6 were conducted in a low-scatter environment with no shield in place. All of these experiments were conducted in the dome of building 470. The geometry of the experiment is shown in figure 4. The scintillators for experiments 3 and 4 were the same as those used in experiments 1 and 2, with  $l = 1.5$  meters for experiment 3, and 0.65 meters for experiment 4. Scintillator selection for experiments 3 and 4 were the same as those used in the first two experiments. For the last two experiments, the BICRON 422 scintillators which measured 2" in diameter and 1" long were replaced by BICRON 404 scintillators which measured 2" in diameter and were 2" long.

The distance from the source to the center of the sensitive volume of the first detector for experiments 3 and 4 was 34 centimeters. Distances between centers of the sensitive volumes of the two detectors were placed at 1.5 meters for experiment 3 and 5 and 0.65 meters for experiments 4 and 6. Several days lapsed before the spectrum generated from each experiment could be used to produce an energy spectrum. Once the time spectrum was

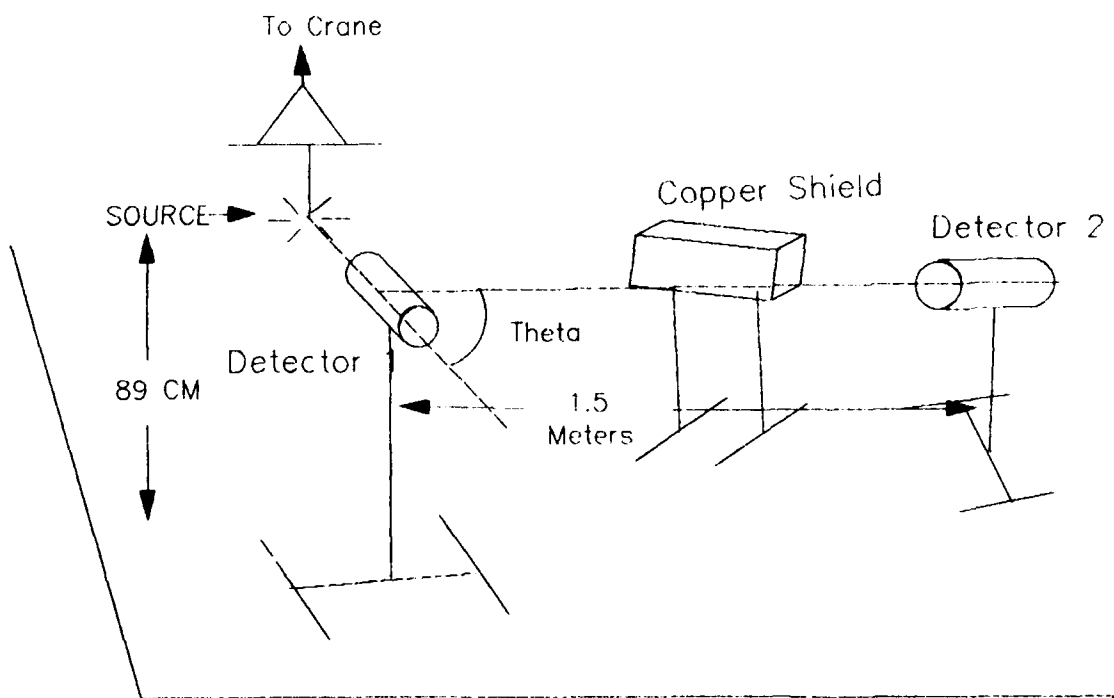


Figure 5. Experiment 3-6 Geometry

generated, it was once again smoothed using the same procedure previously identified. Experiment 4 was identical to experiment 2 with the exception of the location of the experiment itself.

Following the completion of experiment 4, the scintillator detectors were exchanged for the 2" X 2" plastic scintillators with the titanium oxide coating.

Experiments 5 and 6 were the same as experiments 3 and 4, with the exception of the new scintillators. The data for experiment 5 did not produce a spectrum which could be unfolded. Analysis determined the reason for this is the spread in the angle  $\theta$ . With the first detector at 34 centimeters from the source, this spread was  $\pm 6^\circ$  which induced an error in the measured neutron energy of  $\pm 20\%$ . With this much variation in the energy of the neutron, the energy spectrum overlapped itself, rendering it useless. To reduce the spread in scatter angle, the first detector was moved to a distance of 1 meter from the source. This reduced the spread of the angle  $\theta$  to  $\pm 3^\circ$  and the error for the energy reduced to less than  $\pm 10\%$ .

To investigate the relationship between the amount of energy deposited in the recoil protons of the first detector to the time-of-flight data a dual parameter experiment was conducted. Experiment 7 investigated the dual parameter analysis of the information being generated. The proton recoil spectrum from the first detector was put into the y axis of the analyzer and the time-of-flight data into the x axis. Figure (6) is a

picture of the proton recoil spectrum. The time of flight data, when coincident with the proton recoil data, would generate a count in the z direction of the analyzer. The belief was that the time-of-flight data was proportional to the energy deposited in the first detector. Should a low energy neutron deposit half of it's energy into the first detector, and scattered into and reacted with the second detector, then the small pulse height generated should be in coincidence with the longer time-of-flight. The expected result was the build up of the time-of-flight data along a diagonal of the matrix. This experiment was allowed to run for one week. The results are investigated in the analysis and results portion of the report.

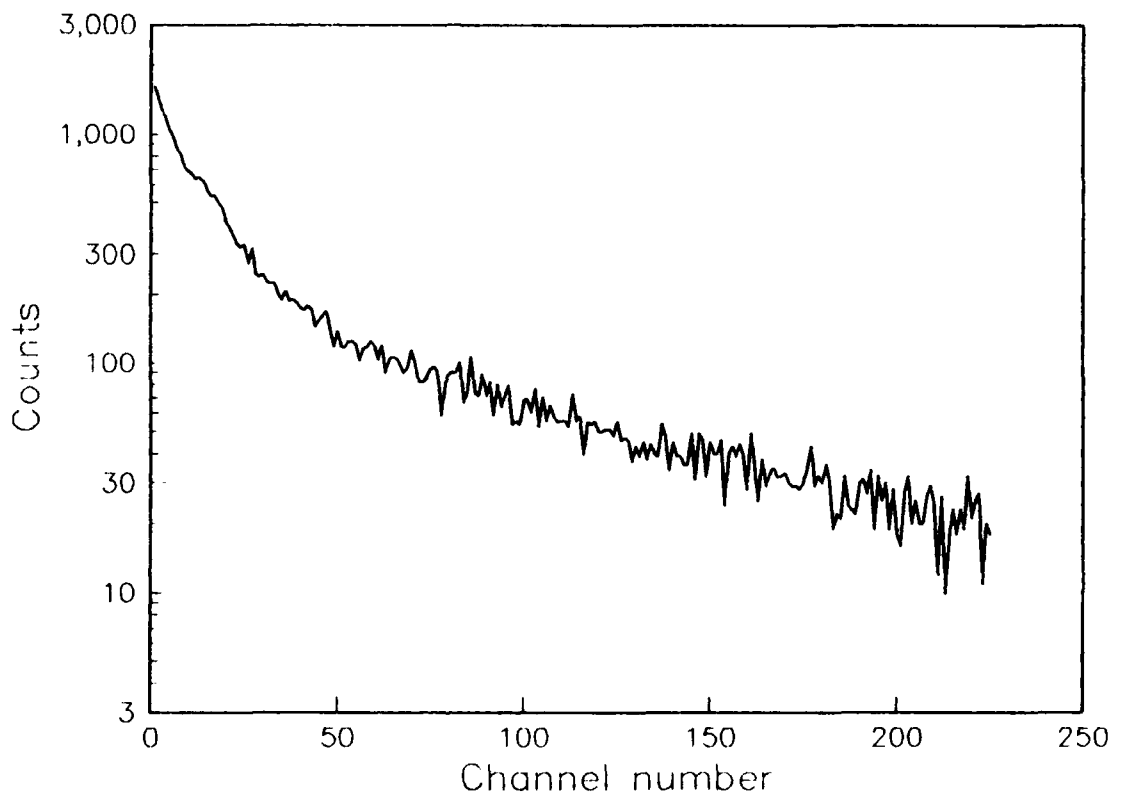


Figure 6. Proton Recoil Spectrum from Detector 1

### III. Analysis and Results

The analysis of the data consists of several phases. First the energy spectra of the different experiments are resolved and compared to the other spectra from other literature. Next, the average energy of the spectrum is calculated by determining the grand mean of the different spectra's average energy. Finally, an error analysis is conducted through the use of a Monte Carlo simulation to determine the energy resolution of the spectrum. To ensure the linearity of the Time-to-Pulse-Height converter, the calibration was conducted prior and following each experiment. In all cases the value of the calibration equation did not change from the start of the experiment until the run was completed. Therefore, the assumption of the linearity of the circuitry is valid.

#### Spectral Data

The published data to compare the energy spectrum from the spectrometer was taken out of an article published by Arun Kumar and P. S. Nagaran in 1977 (8:176). Figure (7) is a picture of the energy spectrum they published. From

this normalized spectrum, the peaks at 3.1, 4.5, 6.5, 7.7, and 9.7 MeV are readily distinguishable. The dip at 6.1 MeV is also a notable feature of the spectrum.

In the high scatter environments of experiment 1, the resolution of the time spectrum took a week to develop. The time spectrum was slow in that the number of incident neutrons on the second detector was 0.17 neutrons per scatter neutron from the first detector. This value was determined analytically by taking the solid angle of the scatter from the first detector to the second detector and determining the total number of neutrons incident on the second detector from a  $4\pi$  scatter. The massive scatter contribution of the environment where the experiment was located initially generated a large low-energy spectrum which did not match the spectrum in figure (7). The shadow shield helped reduce the amount of scatter and the experiment continued. The time spectrum from the analyzer is shown in figure (8). The times for the different channel numbers are obtained by use of the calibration equation for the experiment. This calibration is done using the procedure described in Appendix B. Following the calibration the analyzer gives a slope and y intercept for the calibration equation. A typical equation for the experimental set-up had a negative slope and a y intercept

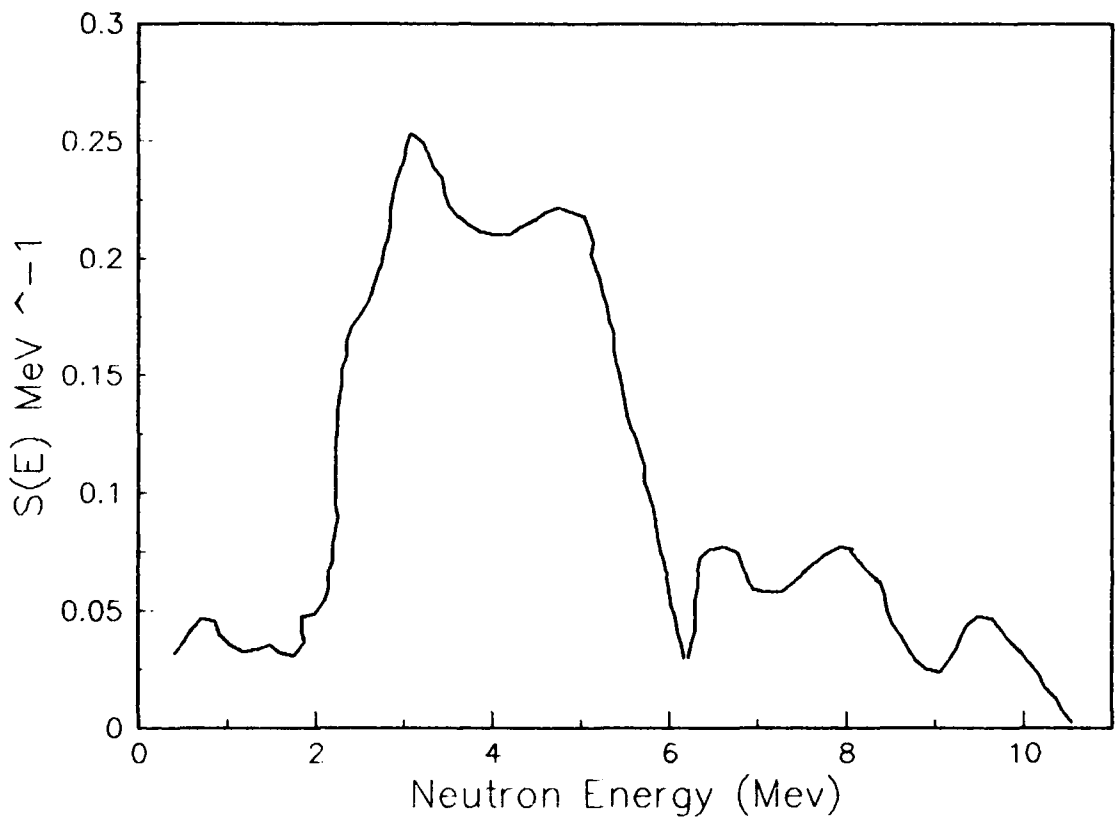


Figure 7. Published Energy Spectrum of a 5 Curie  $^{239}\text{Pu}$ -Be Source by Arun Kumar and P. S. Nagarajan

close to the value of the delay selected for the signal from the first detector. The time for each channel  $\Delta t$ , could then be calculated using the calibration equation.

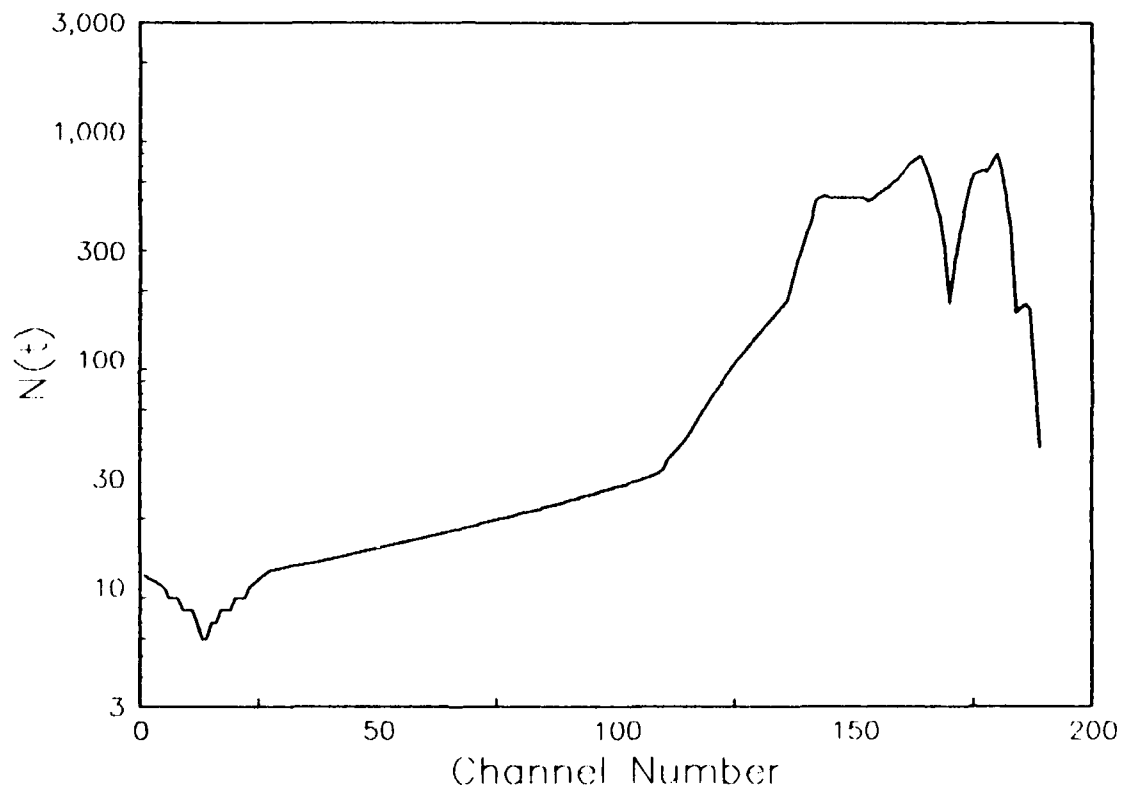


Figure 8. Time Spectrum for Experiment 1

A TK Solver Plus model was used to resolve the time spectrum into the energy spectrum. This model consisted of developing a normalized spectrum from the time spectrum by dividing the individual components of the spectrum ( $n(t)$ ) by the integral of the time spectrum from 0 to  $\infty$ .

$$S(\Delta t) = \frac{n(t)}{\int_0^{\infty} n(t) dt} \quad (25)$$

With the normalized components of the time spectrum  $S(\Delta t)$ , the values of the energy spectrum could be calculated using the results from equation (21). Figure (9) is the normalized energy spectrum resolved from experiments 1 and 2.

As depicted, the locations of the peaks and valleys for the resolved energy spectrum are close to those in figure (8). There are slight differences in the values for the fractional amount in each section of the spectrum. These differences are probably caused by the high scatter environment which contaminated some portions of the data resulting in this poor resolution.

Experiments 3 and 4 resulted in a better energy resolution spectrum, due to the elimination of most of the

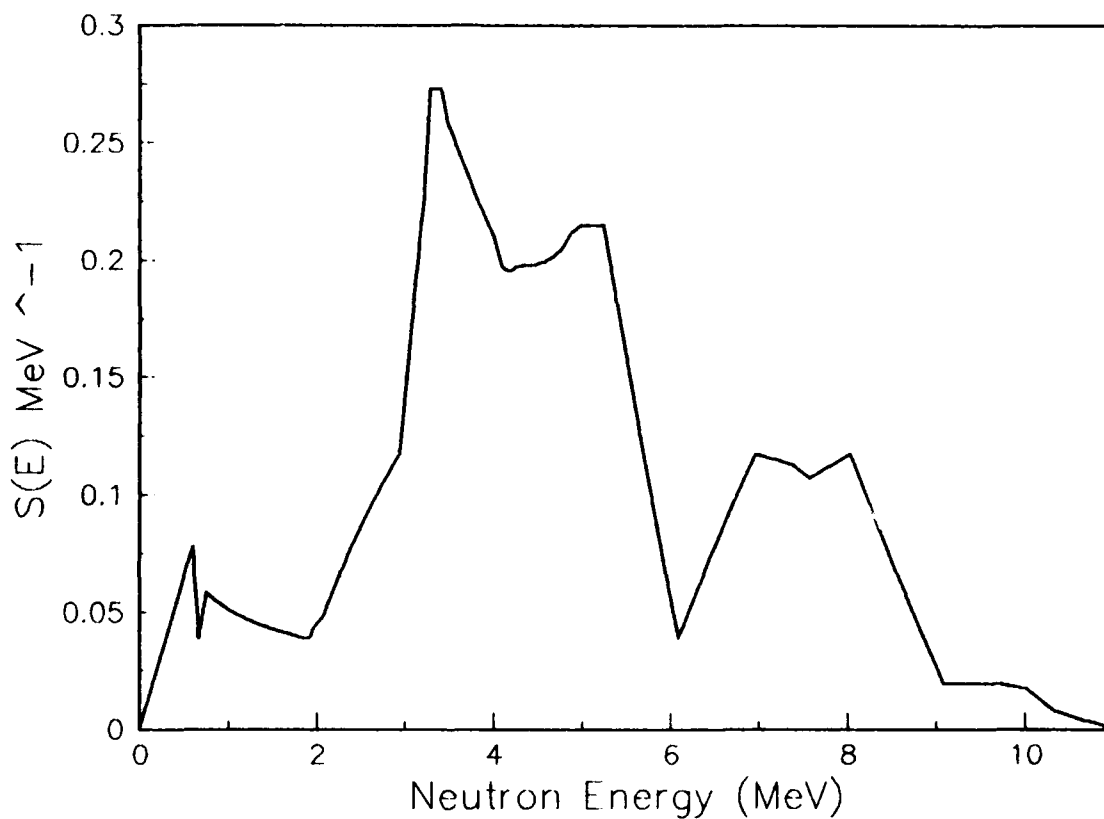


Figure 9. Normalized Neutron Energy Spectrum from Experiments 1 and 2

scatter contribution from the concrete walls. Figures (10) and (11) show the time and resolved energy spectra

produced from experiment 3. The peaks for the different energy resolution in the time spectrum are marked for clarity.

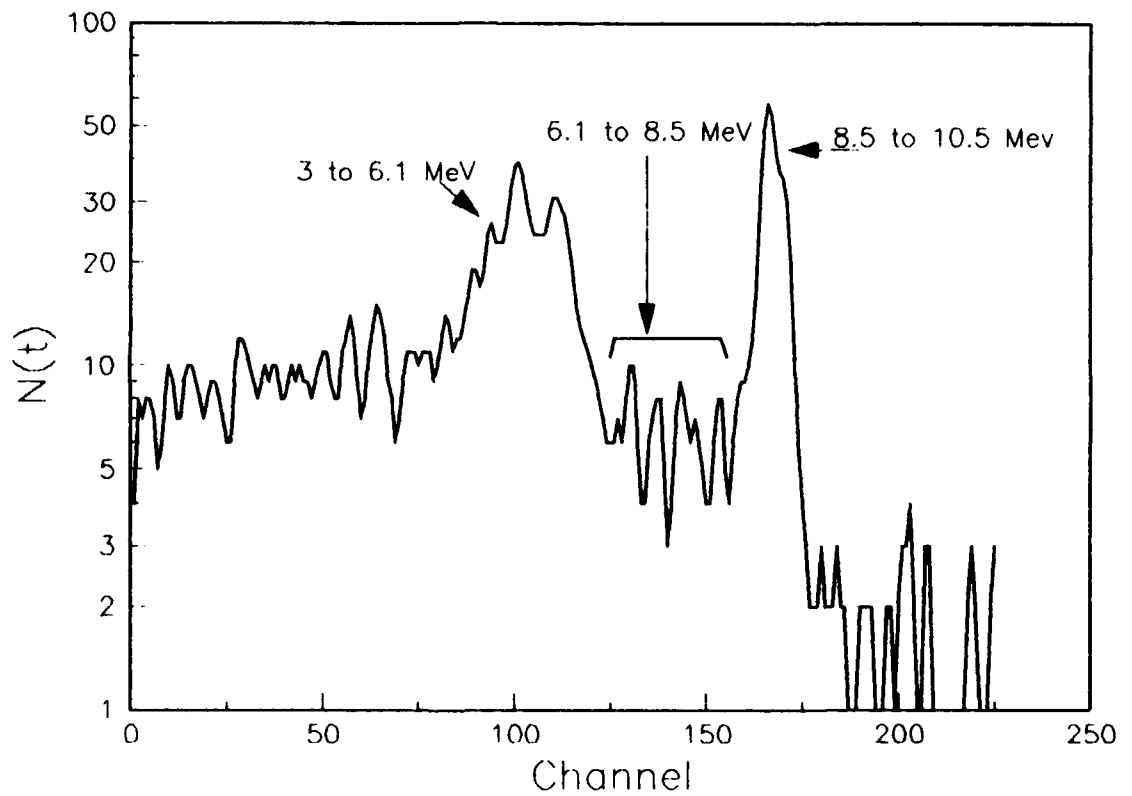


Figure 10. Time Spectrum for Experiment 3

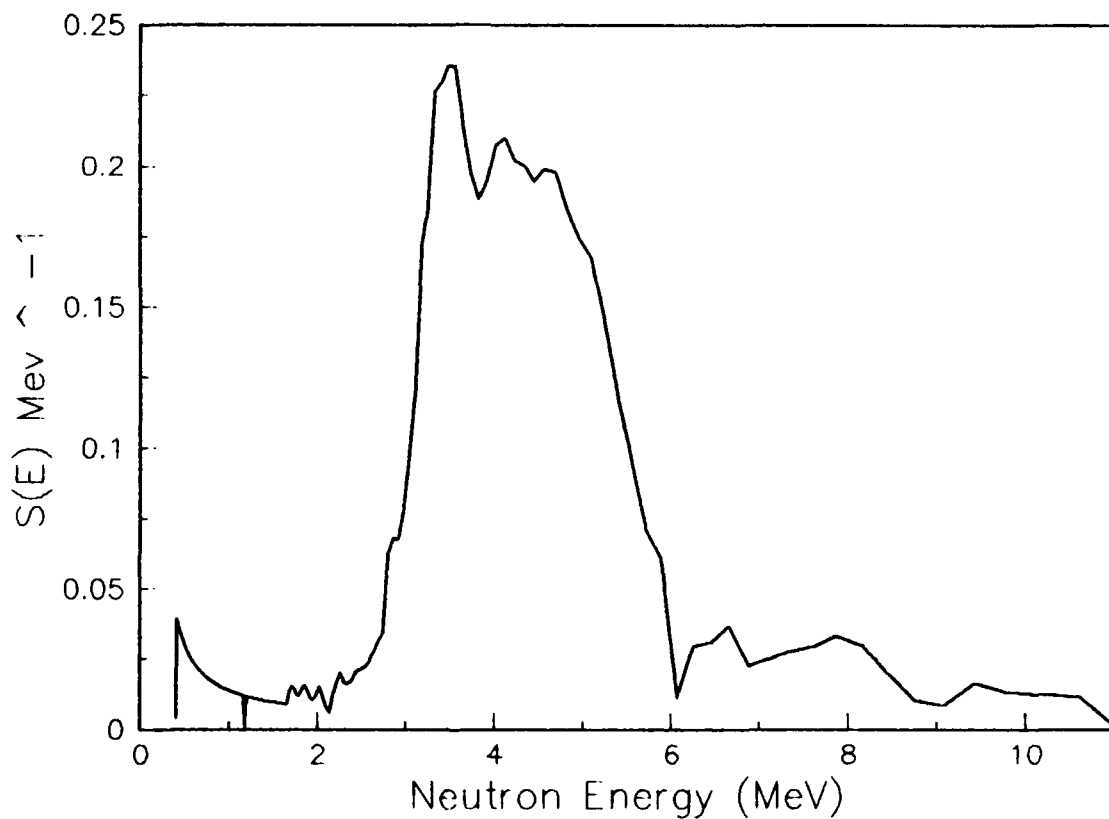


Figure 11. Neutron Energy Spectrum for Experiment 3

Analysis of the energy spectrum indicates the peaks and valleys match the published literature values. The peak at 3.2 MeV is of the appropriate fractional quantity;

however, the spectrum still continues to 11 MeV rather than 10.5 MeV. The origin of this error is still uncertain but believed to have been caused by the arrival in the second detector of scattered neutrons immediately after the excitation of the first detector by an incident neutron. Experiment 4 resulted in no appreciable difference in the resolved energy spectrum. Following this experiment, the scintillators were changed and the system allowed to stabilize for twenty-four hours.

Experiment 5 indicated that the number of interactions in the first detector increased by a factor of 2.5 over that of the first scintillators. This is due to the doubling of the hydrogen atoms, which would cause the reaction rate of the incident neutrons to double, and the doubling of the path length which the neutrons travel through the medium which increased the intrinsic efficiency of the detectors. Interactions in the second detector increased by a factor of five. After two days, the time spectrum from the experiment did not evolve as the ones from the previous experiments. Investigation revealed the spread in the scatter angle to be large. This spread was from 0.7 radians to 0.907 radians which induced a large error in the resolution of the energy spectra. With this large of a spread in  $\theta$ , the time

resolution disappeared, generating a spread in time for a 5.25 MeV recoil neutron to vary from 62.34 nanoseconds to 77.16 nanoseconds.

To correct this, the first detector was placed 1.0 meters away from the center of the source. When the experiment was repeated, the spread in the scatter angle and time reduced. The values for the spread in scatter angle went from the values previously mentioned to 0.75 to 0.84 radians, and the time spread reduced to 65.0 to 71.0 nanoseconds. The time resolution reappeared and the energy spectrum resolved into Figure (12).

To compare the obtained data to the published spectrum, the spectrum in figure 6 was overlaid as shown in Figure (13). The plot indicates that the spectrum between 3 and 6 MeV did not correspond with that in the literature. The dip at 6.1 MeV occurs at 5.9 MeV, and the fraction of neutrons between 2 and 3 MeV are not of the appropriate values. Neutron distribution between 6 and 10.5 MeV, however, are virtually the same as the one published. Experiment 6 demonstrated the same spectrum as experiment 5 with no improvement over the resolved energy spectrum. This error is caused by the energy resolution from the spread in the scatter angle  $\theta$ , and the error induced by the scatter of neutrons in the

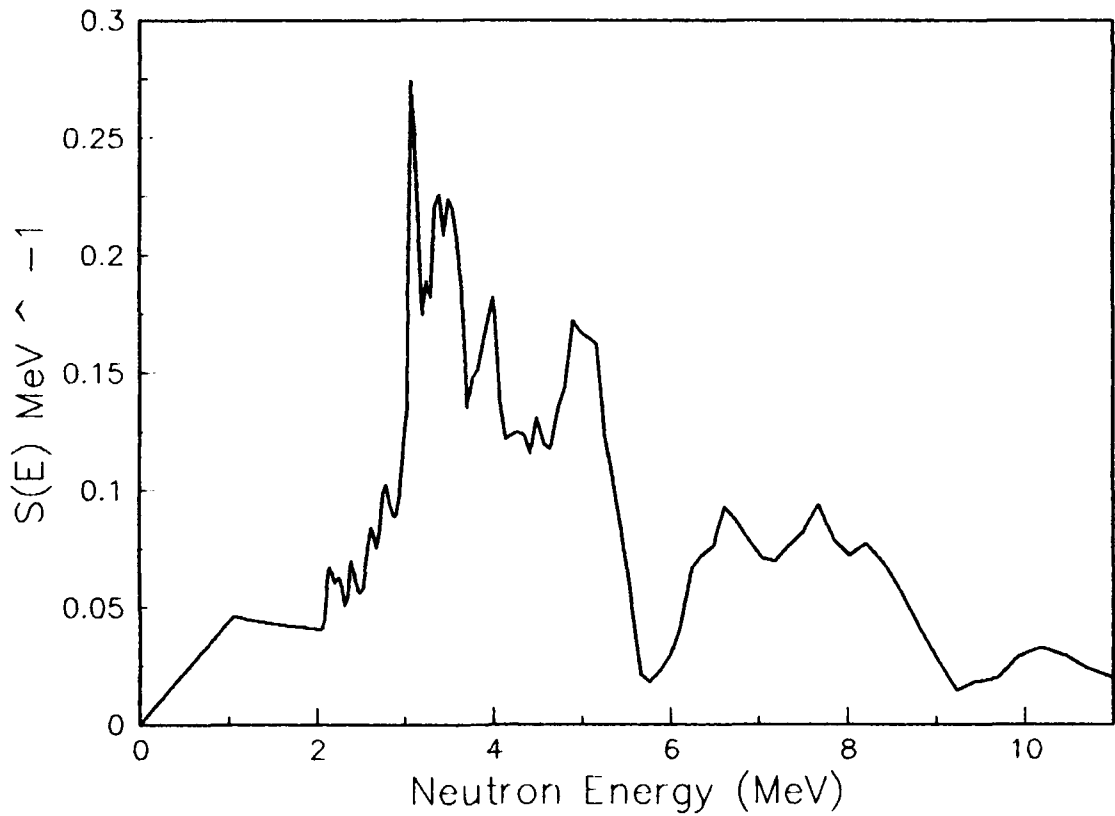


Figure 12. Experiment 5 Neutron Energy spectrum

surroundings.

To conduct the dual parameter experiment, several factors had to be implemented. The first was to generate

and attempt to calibrate the proton recoil spectrum from the first detector and place them in coincidence with the time-of-flight data. This spectrum is seen in Figure (6). Calibration of the proton recoil spectrum was not accomplished due to the lack of a mono-energetic neutron source below 10 MeV. Therefore, the experiment was conducted without calibration.

The set up on the dual parameter analyzer was as follows: the time-of-flight data was put into the first channel of the analyzer, and the proton recoil spectra was placed on the second channel. A coincidence window of 0.2 micro seconds was used to generate the data. The grid was set up to be a 64 X 64 matrix. If a time-of-flight pulse should occur during the coincidence window of a proton recoil, then the analyzer would generate a count at that point. To ensure that the timing was correct for the proton recoil spectra, the signal from the linear amp of the first detector was delayed the same amount of time as the anode signal from the first detector. Figure (14) is a picture of the analyzer screen following a week of data collection.

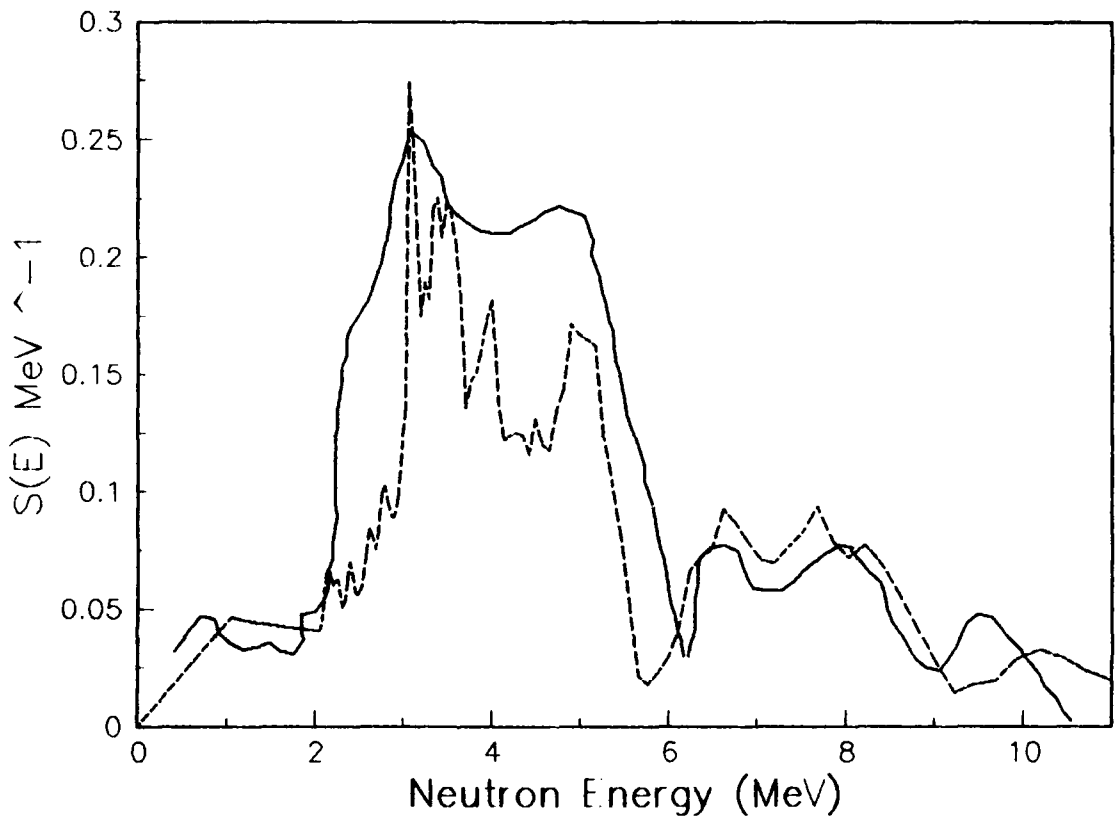


Figure 13. Comparison of Published Data with Experimental Data

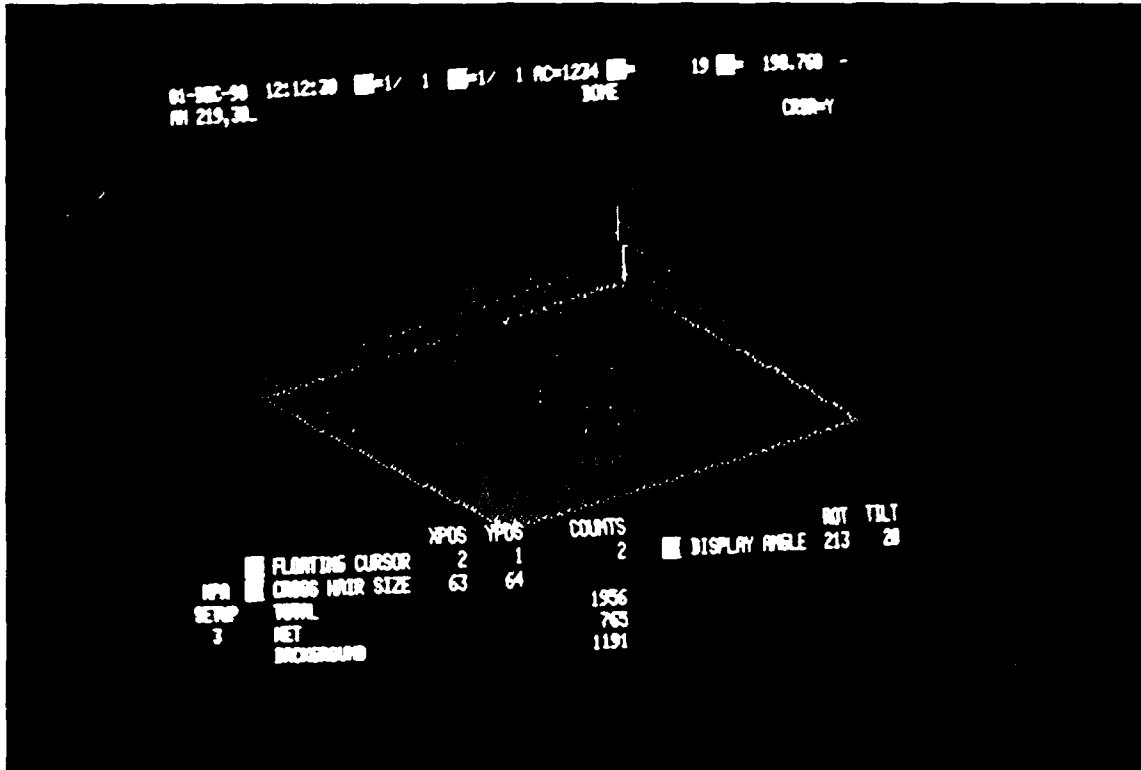


Figure 14. Experiment 7 Dual Parameter Analyzer Display

To understand the plot, the following information is needed. From the upper right corner of the plot, the time-of-flight information is along the axis going to the left and the proton recoil spectra is on the right axis.

As shown in this picture, the more energetic neutrons produce the longer flight time and generate the first peaks from the left. The coincidence window of 200 nanoseconds resulted in the generation of a lot of spurious pulses in the lower ranges under this peak, thus reducing the readability of the plot. The time-of-flight data can be determined, however, by looking at the highest proton recoil energy of each time-of-flight peak. If this is accomplished, the spread of the time-of-flight data corresponds to that previously predicted. The neutrons deposit half of their energy,  $(\cos^2(\frac{\pi}{4}))$ , into the hydrogen atom. Therefore the lower the energy of the neutron incident on the first detector, the longer the time-of-flight would be. Realizing the time spectrum is backwards for the time-of-flight data, i.e. channel 1 = 200 nanoseconds, channel 256 = 0 nanoseconds, the plot starts to come together. Additional studies, however; need to be accomplished to reduce the spurious pulses from the time-of-flight axis.

### Average Energy

To compute the average energy of the different spectra, the first moment of the spectra was divided by the zeroth moment.

$$E_{avg} = \frac{\int_0^{\infty} ES(E)dE}{\int_0^{\infty} S(E)dE} \quad (26)$$

This integration was accomplished numerically, and the grand mean of the average values of the different energy spectra was determined to be  $4.6 \pm 0.1 \text{ MeV}$ . This value is the same value obtained from the spectrum in figure (6).

To calculate the average efficiency for the detector system the average path length for the neutron travel in the different detectors was taken as 2.54 centimeters for experiments 1-4, and 5.08 centimeters for experiments 5 and 6. Using the value for the average energy previously obtained, and equations (22) and (23), the average efficiency for the detectors was calculated to be  $0.1 \pm 0.02$  for experiments 1-4 and  $0.2 \pm 0.02$  for experiments 5 and 6.

## Error Analysis

The error analysis for the experimentation undertaken proved to be very difficult. From a single deviation in the amount of time, length of travel, and scatter angle, the errors needed to be propagated from equation (9) through equation (21). Even if Poisson statistics are assumed, the propagation of the various errors was insurmountable. The energy resolution is the main concern and to determine the spread in this value the scatter angle spread must be known.

Defining the scatter angle,  $\theta$ , consumed a large portion of the analysis phase of this project. For the first two experiments, the spread of  $\theta$  was 0.1 radians and 0.14 radians, respectively. These values were obtained through the error analysis performed by using a Monte Carlo simulation routine.

The Monte Carlo simulation routine established for the error analysis was constructed through the use of a TK Solver model. A copy of this model is listed in Appendix C. This model took 1000 random points for each of the following: (1) the place of the neutron generation in the source; (2) place for the scatter in the first detector; and (3) place for the interaction in the second detector.

Then for the same time of flight,  $\Delta t$ , the energy of the neutron incident on the first detector was calculated. Accomplishments of this was undertaken by generating non-nominal distances of flight and scatter angle,  $\theta$ . With these values, the energy of the scattered neutron could be calculated based on the distance traveled and the time it took to traverse this distance (constant). The scatter angle determined for this event, and the energy of the incident neutron calculated through the use of equation (22). The details of the sampling method employed in the error analysis model follows.

To sample the probability of the location of the different events the use of a probability distribution function was needed. In order to generate this function, the probability of an interaction was taken to be that of a differential area of a cylinder,

$$P(r, \theta, z) dr d\theta dz = r dr d\theta dz \quad (27)$$

Which indicates that the probability,  $P$ , must be proportional to the location of the event in the radius,  $r$ .

To sample the event, inversion of the probability distribution function was necessary. This was

accomplished by taking the ratio of the respective circular areas for the location of the event at radius,  $r$ , to that of the circular area of the entire radius,  $R$ , and setting this value equal to a random number  $\xi$ .

$$\frac{\pi r^2}{\pi R^2} = \xi \quad (28)$$

or simply,

$$\frac{r^2}{R^2} = \xi \quad (29)$$

Therefore, by use of cylindrical geometry, the value of the sampled radius of the event,  $r$ , the angle  $\theta$ , and height,  $z$ , are given by:

$$\begin{aligned} r &= R\sqrt{\xi} \\ z &= h\xi \\ \theta &= 2\pi\xi \end{aligned} \quad (30)$$

where  $R$  is the radius of the different components, and  $h$  is the height of the different components.

The value of  $\xi$  for the  $z$  component is computed a little differently than just from the generation of a random number. Because the flux of neutrons will decay

exponentially through the sensitive volume of the detector, the random number must be biased toward the front of the detector. To accomplish this task, the cumulative distribution function

$$C. D. F. = (1 - \exp(-\sigma d)) \quad (31)$$

is used to determine the value of interaction within the volume  $d$ , where  $d$  is generated by taking the negative of a natural log of a random number divided by the value of the macroscopic cross section  $\sigma$ . Once this value is known the value of  $\xi$  is determined.

With the different points established for the different events, the analysis of the energy resolution could begin. To accomplish this, the initial data for the six experiments was placed in the Monte Carlo routine. The times selected for analysis corresponded to the fastest neutron, 10.5 MeV, the slowest neutron, 0.5 MeV and the average neutron, 4.6 MeV. The data for the different energies for these times were then sorted using a quick basic routine and the number per group plotted.

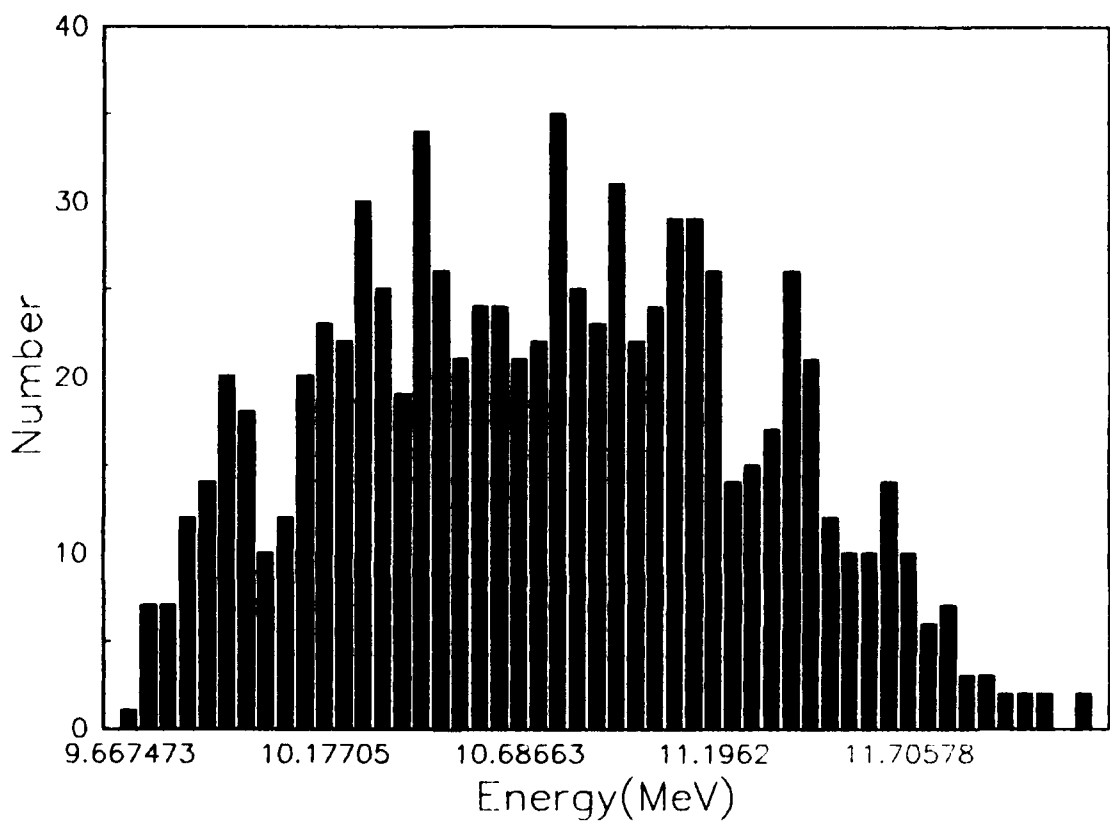


Figure 15. Error Analysis for High Energy Spectrum

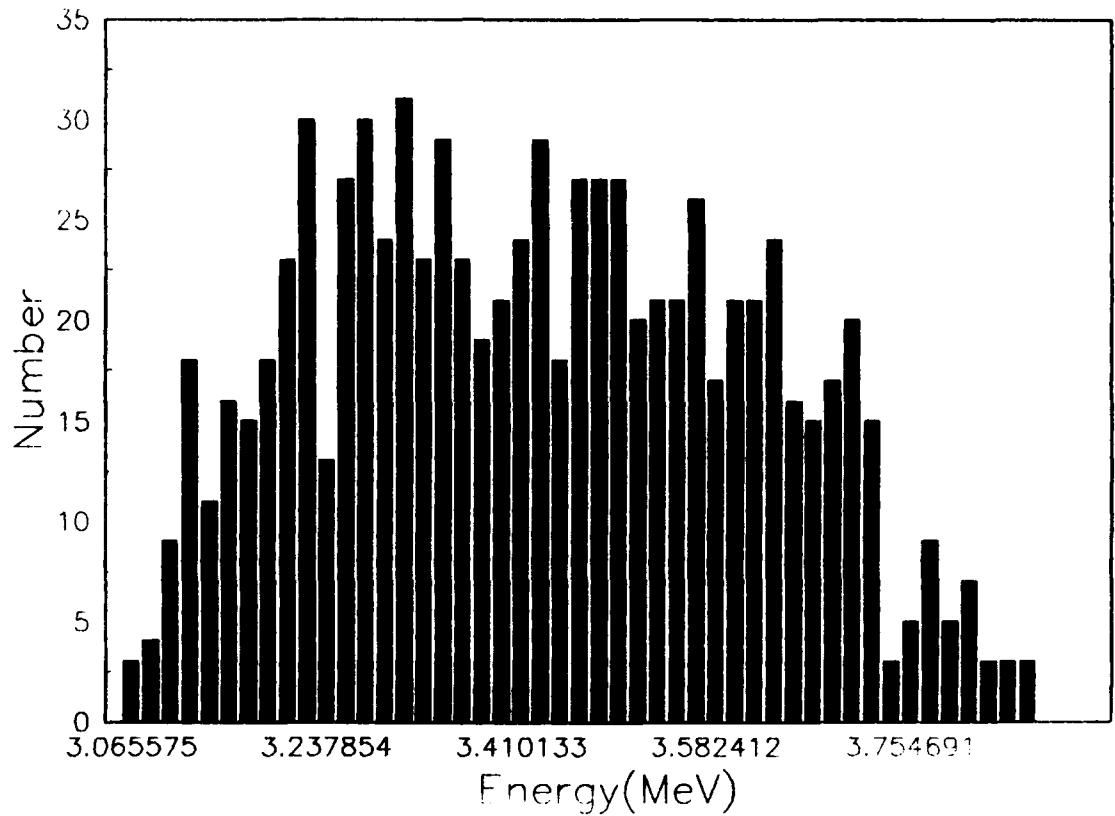


Figure 16. Error Analysis for Mid-Range Neutron Energy

Analysis of the data in figures (15-17) indicates that the average energy of the high energy spectrum  $\Delta t$ , is given as  $10.85 \pm 0.34$  MeV, for the mid range as  $3.4 \pm 0.04$  and for the low end  $1.07 \pm 0.005$ . A similar analysis was

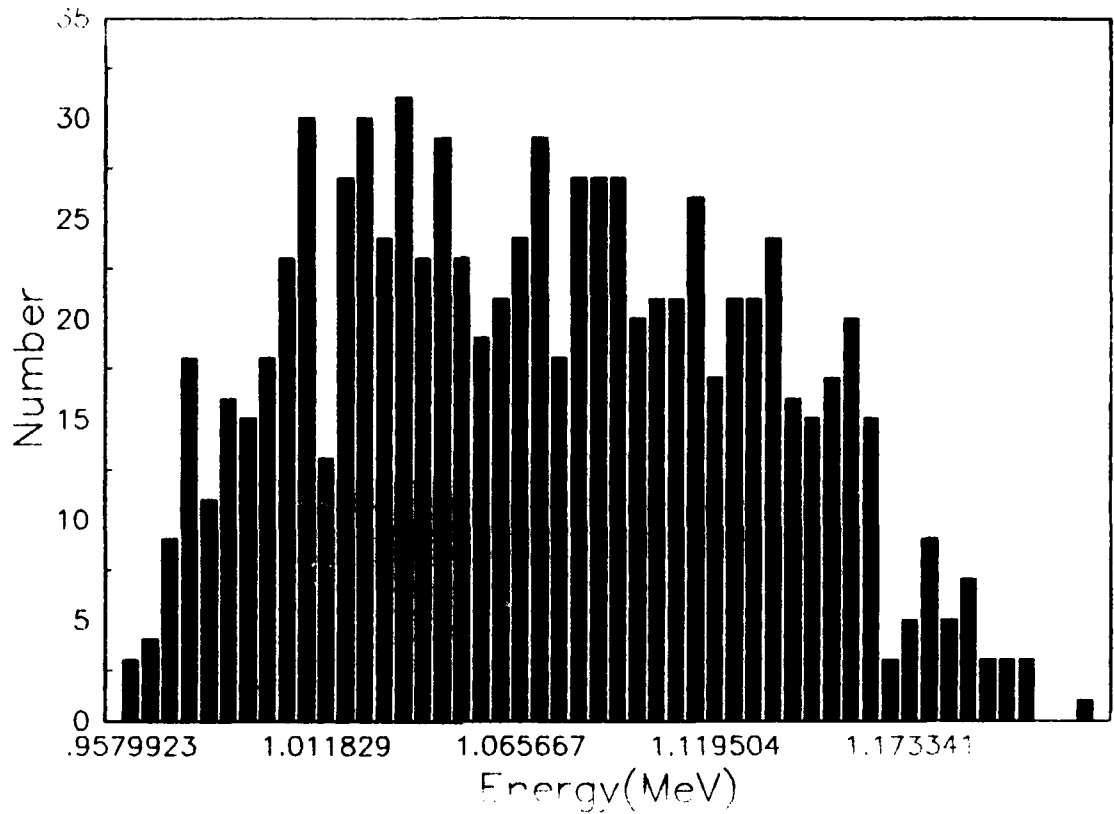


Figure 17. Error Analysis for Low Energy Neutron

accomplished for the value of  $\theta$ , and length  $l$ . It was assumed that  $\theta = 45^\circ$  for the analysis. The values obtained for the different components were  $\theta = 45.2^\circ \pm 0.2^\circ$  and  $l = 1.51 \pm 0.01$  meters.

#### IV. Discussion, Conclusions and Recommendations for Future Studies

Energy spectrum from a  $^{239}\text{Pu}$ -Be source was determined by using a neutron time-of-flight spectrometer. This spectrometer measures the time of flight of the neutron between two points and generates a corresponding time spectrum. The time spectrum was unfolded into the energy of the incident neutron through the use of a TK Solver model. Energy spectrum which were generated from the time spectrum were compared to those in the literature. Several experiments were undertaken to investigate the effect that the distance between two detectors,  $l$ , had on the energy resolution along with the effect of two different scintillators. The two values of  $l$  investigated were 0.65 meters and 1.5 meters. Scintillators of 2" in height were replaced for ones with 1" height and the different energy spectra considered. Additionally, the effect of the high-scatter environment contributed to the building of a shadow shield in order to prevent the scattered neutrons from the walls and floors to corrupt the data. Elimination of this nuisance was accomplished by moving to a low scatter environment.

Uncertainty in the time spectrum can be from a number of sources. Definition of the scatter angle,  $\theta$ , along with the

determination of the true path length of flight are the largest contributors. Multiple scatters of the neutron with hydrogen or even the carbon atoms can also contribute to the uncertainty in the unfolded energy spectrum.

The last experiment considered the coincidence of the proton recoil energy spectrum to that of the time-of-flight. Even though the results are hazy, the desired effect can be seen. Additional study should be undertaken to resolve the long coincidence window timing problem.

Although several types of spectrometers have been developed to determine the energy spectra of different neutron sources, most have limitations as to the range of energy coverage. The time-of-flight spectrometer has emerged as the preferential choice for determining the energy spectrum from any neutron source. From the time spectrum, which is generated by the time-of-flight spectrometer, the energy spectrum is easily achieved through the use of manipulation of the kinematics equations and distribution functions. The error analysis of the energy resolution which is not readily obtainable from the propagation of errors through the equations, can be accomplished by use of a Monte Carlo simulation.

Neutron spectrum obtained from a 5 curie Pu-Be source with the time-of-flight neutron spectrometer are approximately

as described in the literature. They take a long time to obtain with "weak" sources when just two detectors are used. A low-scatter environment is essential although some results are possible in a high-scatter environment if appropriate shielding is used. Refinements are required to improve the resolution of the time spectrum, such as defining the dependence of  $\theta$  on the different geometries available. Another avenue to investigate would be the use of a small scintillator on the first detector, and a large scintillator on the second detector. This would allow the placement of the first detector closer to the source, increasing the number of neutrons incident on it, without losing the definition of the scatter angle. The larger scintillator on the second detector would improve the efficiency of the second detector and reduce the amount of time necessary to generate the time spectrum. Again consideration must be given to the scatter angle spread.

The average energy for the neutron source selected is  $4.6 \pm 0.1$  MeV which is the same value from the spectrum given by Arun Kumar and P. S. Nagarajan. With this value for the average energy, the intrinsic efficiency of the detectors is determined to be around 0.1 - 0.2. This efficiency increases with an increase in the volume of the sensitive volume and an increase in the average path length of travel.

Further studies should be undertaken to improve the resolution of the time spectrum, and thus the energy spectrum of the source. One modification could be the placement of the second detector at a distance of 3.0 meters from the first detector with the first detector at a distance of 2.0 meters from the source. This would allow for the spread in the scatter angle,  $\theta$ , to be minimized. A second study should be undertaken to refine the dual parameter aspect. By placing a greater distance between the detectors, the resolution of the coincidence events could be better understood. The minimum coincidence window for the dual parameter analyzer is 0.1 microseconds and the average time of flight for the neutron between the detector should be at least an order of magnitude greater than this. The use of several detectors in an array a fixed distance from the first detector which would generate the same scatter angle would reduce the amount of time necessary to generate the time spectrum.

### Appendix A. Equipment list

The following is a list of equipment used to establish the spectrometer circuit for the time-of-flight system.

<u>ITEM</u>	<u>MANUFACTURER</u>	<u>MODEL NUMBER</u>	<u>ID NUMBER</u>
Photomultiplier Tube	RCA	8575	P52180 T30499
Photomultiplier Base	Ortec	265	1589 1592
Plastic Scintillator	Bicron	422 (Exp 1-4) 404 (Exp 5-7)	none none
Preamps	Ortec	113	6511 6571
Linear Amps	Ortec	572	0978 4745
Quad CFD	Tennelec	TC 454	509
Gate and Delay Generators	Ortec	416A	3640 3639 3679

<u>ITEM</u>	<u>MANUFACTURER</u>	<u>MODEL NUMBER</u>	<u>ID NUMBER</u>
Timing SCA	Ortec	551	2755 2768
Timer/Counter	Ortec	996	116 125
Pulse Shape Analyzer	Ortec	458	567
Delay Amp	Ortec	463	832
Time to Amplitude Converter	Tennelec	TC-873	244
Fast Coincidence Circuit	Ortec	414A	810
Time Calibrator	Ortec	462	390
High Voltage Power Supply	Ortec	556	1993

<u>ITEM</u>	<u>MANUFACTURER</u>	<u>MODEL NUMBER</u>	<u>ID NUMBER</u>
Oscilloscope	Tektronics	425	3465
NIM Bins	Ortec	4001C	3583 3520
Dual Parameter Analyzer	Nuclear Data	ND 76	963085
Neutron Source	Monsanto	Pu-Be	M1170

## Appendix B. Timing and Calibration Procedures

The following procedure was used to time the circuitry and the calibrate the time to amplitude converter for use in the spectrometer.

1. Place both detectors equal distance from neutron source.
2. Feed inputs to the fast coincidence circuit from detector 2 to the dual channel oscilloscope. Select triggering mode to channel one or channel 2.
3. Adjust gate and delay circuits until pulses are in coincidence on scope.
4. Re-attach cables to inputs of fast coincidence circuit; set resolving time to 100 nanoseconds.
5. Check output of fast coincidence circuit; should be positive logic pulse. If not repeat steps 2-4.
6. Remove all delays from detector 1 anode circuit.
7. Place start and stop signals from the time to amplitude converter to the dual channel oscope.
8. Adjust gate and delay circuit of the anode signal from detector 1 only to bring signals into coincidence; trigger oscope on start signal from detector 2.
9. Insert fixed delay into anode signal from detector 1.
10. Re-attach start and stop signals to time to amplitude

converter.

11. Select range scale on time to amplitude converter to match fixed delay set in step 9.
12. Place multiplication plot to 1.25.
13. Check to see that you have valid conv lite; tac out lite; and SCA lite on.
14. Remove the start and stop signals from the time to amplitude converter.
15. Place the start and stop signals from the time calibrator into the start and stop in connections of the time to amplitude converter.
16. Select range on the time to amplitude converters to a value just under the fixed delay selected for the anode circuit from detector 1.
17. Select period setting to 20 nanoseconds.
18. Acquire data from time to amplitude converter on dual parameter analyzer.
19. Using RM and LM commands place right and left markers on the peaks generated by the time to amplitude converter.
20. Determine the value of the right peak and left peak by subtracting the value of the range determined in step 16 from the fixed delay in the anode circuit of detector 1; this is the value of the right marker energy.
21. The other peaks will be every 20 nanoseconds apart,

increasing from right to left, instead of left to right.

22. Use the calibration commands LE and RI and place the value of the peaks for the left and right markers into the dual parameter analyzer.

23. Remove the start and stop signals from the time calibrator and reconnect start and stop signals from spectrometer circuit.

24. Reestablish geometry for experiment and commence experiment.

### Appendix C. TK Solver Models Used for Analysis

The following model is the one used to resolve the time spectrum into the energy spectrum. To accomplish this the model first generates a normalized time spectrum and then uses equation 17 to generate the energy spectrum. This spectrum is then analyzed for the average energy by taking the value of the first moment of the spectrum over the zeroth moment of the spectrum. The function for integration is a list function with cubic interpolation between the data points.

#### Variable Sheet

St	Input	Name	Output	Unit	Comment
		E		Joules	recoil neutron energy
		Er		MeV	recoil neutron energy
	1.627E-27	m		Kg	mass of neutron
		v		m/sec	velocity of neutron
	1.5	l		meters	distance between det 1 and det 2
		deltat		sec	time of travel
	0	Ch			channel number

	st		sec <sup>-1</sup>	normalized time spectrum
0	nt			time spectrum
0	Se		MeV <sup>-1</sup>	Energy spectrum
0	En		MeV	Incident Neutron Energy
45	theta		degrees	Scatter angle
	Num	.12722		Value of first moment
0	low			smallest value of energy
11	high			highest value of energy
	Den	.035327		Zeroth moment
	Eavg	3.60124		Average Energy of spectrum
1000	div			Number of bins for numerical integration

Rule-----

- \*  $E_r = E/1.602e-13$  " Converts from Joules to MeV"
- \*  $E = .5*m*v^2$  "Kinematics Equation for Kinetic Energy"
- \*  $v = 1/deltat$  "Definition of velocity"

```

* deltat = (-.8*Ch+196.8)*e-9      "Calibration equation for
                                   experiment

* st = nt/sum('nt)                "Determines s(t) from n(t)

* Se = st*(deltat^3)/(m*1^2)      "Determines s(e) from s(t)"

* Er = (cosd(theta))^2*En         "Determines neutron energy from
                                   recoil energy"

* Num  Fmom(low,high)              "Determines first moment for
=                                     spectra using trapezoid rule"

* Den  Trap(low,high)             "Determines zeroth moment for
=                                     spectra using trapezoid rule"

* Eavg = Num/Den                  "Determines avg energy"

```

The second model used is the error analysis model. To determine the error in the energy spectrum, the random number,  $\xi$ , is used along with equation 26. The zero plane for the z axis is the bottom of the neutron source, whereas the zero plane for the y axis is the bottom of the first detector's sensitive volume and the zero plane for the x axis is the center line of the first detector's sensitive volume.

Using this for the origins we see that the values for the location of the neutron generation in the source (x, y, z) are given by (rcos  $\theta$ , rsin  $\theta$ , z). The values for the neutron reaction (x, y, z) in the first detector are given by (rcos  $\theta$ , z, rsin  $\theta$ ). The last detector has initial coordinates based

on the geometry of the experiment and then the values of the neutron interaction (x, y, z) are given by the initial value of the bottom center of the sensitive volume minus ( $z \cos -\frac{\pi}{4}$ ,  $r \cos \theta \sin -\frac{\pi}{4}$ ,  $r \sin \theta$ ). Values for the time of travel, energy of neutron, and spread in  $\theta$  can be determined. It is important to note that you must input either the energy of the neutron in order to generate a time difference or a fixed time to generate the energy spread.

== VARIABLE SHEET == For Academic Use Only

St Input Name Output Unit Comment

INITIAL PARAMETERS FOR PROBLEM

\*\*\*\*\*

150	LDET1TO	cm	Distance from det1 to det2
100	LSORTOD	cm	Distance from source to det1
1.0414	Rsource	cm	Radius of source
9.488	Zsource	cm	height of source
2.54	Rdet1	cm	radius of det1
2.54	Zdet1	cm	length of det 1
2.54	Rdet2	cm	radius for det 2
2.54	Zdet2	cm	length of det 2
46.904442	deltat	nanosec	Time for travel between det1 and det2
1.675E-27	M	kg	mass of neutron

GENERATE RANDOM VALUES

\*\*\*\*\*

L .2	random		random number
	rsource	cm	random r for source
	zsource	cm	random z for source
	thetaso	radians	random angle for source
	rdet1	cm	random radius for det1
	zdet1	cm	random z for det 1
	thetade	radians	random angle for det 1
	rdet2	cm	random radius for det2
	zdet2	cm	random z for det 2
	thetade	radians	random angle for det 2

CONVERT TO RECTANGULAR COORDINATES

\*\*\*\*\*

xsource	cm	x component of source
ysource	cm	y component of source
ZSOURCE	cm	z component of source

xdet1	cm	x component of det1
ydet1	cm	y component of det1
ZDET1	cm	z component of det1
xdet2	cm	x component of det2
ydet2	cm	y component of det2
ZDET2	cm	z component of det2

CALCULATED VALUES FOR ERROR

ANALYSIS

\*\*\*\*\*

	lendet1	cm	Length det1 to det2 for neutron travel
L	.76492326	theta	radians Scatter angle
	E1	MeV	recoil energy of neutron
L	10.168283	En	MeV Incident neutron Energy

MINIMUM AND MAXIMUM VALUES  
FOR ANALYSIS

\*\*\*\*\*

	minimum	MeV	Minimum value of En
	maximum	MeV	Maximum value of En

	Minthet	radians	Minimum theta(scatter angle)
	Maxthet	radians	Maximum theta(scatter angle)
	minleng	cm	minimum length travel
	maxleng	cm	maximum length travel
	mintime	nanosec	minimum time for travel
	maxtime	nanosec	maximum time for travel
	.78875847 thetaav	radians	average theta
L	thetasp	radians <sup>2</sup>	intermediate term needed for spread
	thetava .00042376	radians <sup>2</sup>	variation of theta
	10.84695 nbar	MeV	average of data
L	ssqddat	MeV <sup>2</sup>	data for s <sup>2</sup>
	ssqd	MeV <sup>2</sup>	s <sup>2</sup>
			intermediate values necessary for generation of data
*****			
	v	m/sec	velocity of recoil neutron
	thetaso		angle source to det 1
	thetade		angle det1 to det 2

seed2		random # generated
seed3		random # generated
seed4		random # generated
seed5		random # generated
seed6		random # generated
seed7		random # generated
seed8		random # generated
seed9		random # generated
seed10		random # generated
totalE	MeV	

10.168283 Eavg1	barns	Average Energy of spectrum
.91257036 sigmas1	MeV	microscopic cross section for
Hydrogen		
.04754492 Sigmas1	cm <sup>-1</sup>	Macroscopic cross section
21.032743 Lambda1	cm	atomic density for hydrogen
1.521548 sigmas	barns	microscopic cross section for
Hydrogen		
5.2922779 Eavg	MeV	Average Energy of spectrum
.07927265 Sigmas	cm <sup>-1</sup>	Macroscopic cross section
5.21E22 Nh	atoms/cm <sup>3</sup>	atomic density for hydrogen
12.614691 Lambda	cm	mean free path for det2

== RULE SHEET == For Academic Use Only

S Rule

---

seed2=SEED1(random)

rsource=Rsource\*(Xi(seed2))^.5

seed3=SEED1(seed2)

zsource=Zsource \* Xi(seed3)

seed4=SEED1(seed3)

thetasource=2\*pi()\*seed4

seed5=SEED1(seed4)

rdet1=Rdet1\*(Xi(seed5))^.5

seed6=SEED1(seed5)

zdet1=Zdet1\*zdet(seed6,Sigmas1)

seed7=SEED1(seed6)

thetadet1=2\*pi()\*seed7

seed8=SEED1(seed7)

rdet2=Rdet2\*(Xi(seed8))^.5

seed9=SEED1(seed8)

zdet2=Zdet2\*zdet(seed9,Sigmas)

seed10=SEED1(seed9)

thetadet2=2\*pi()\*seed10

xsource=rsource\*cos(thetasource)

$y_{source} = L_{SORTO}DET1 + r_{source} * \sin(\theta_{source})$

$Z_{SOURCE} = z_{source}$

$x_{det1} = r_{det1} * \cos(\theta_{det1})$

$y_{det1} = z_{det1}$

$Z_{DET1} = .06908 + r_{det1} * \sin(\theta_{det1})$

$x_{det2} = (L_{DET1}T_{ODET2} + Z_{det2}) * \cos(-\pi()/4) - z_{det2} * \cos(-\pi()/4)$

$y_{det2} = (L_{DET1}T_{ODET2} + Z_{det2}) * \sin(-\pi()/4) + r_{det2} * \cos(\theta_{det2}) * \sin(\pi()/4)$

$Z_{DET2} = .06908 + r_{det2} * \sin(\theta_{det2})$

$\theta_{det1}t_{odet2} = \text{ABS}(\text{atan2}(y_{det1} + y_{det2}, x_{det1} + x_{det2}))$

$\theta_{source}t_{odet1} = \text{ABS}(\text{atan2}(y_{det1} + y_{source}, x_{det1} + x_{source}))$

$\theta = \pi() - (\theta_{source}t_{odet1} + \theta_{det1}t_{odet2})$

$l_{endet1}t_{odet2} = ((x_{det1} + x_{det2})^2 + (y_{det1} + y_{det2})^2 + (Z_{DET1} + Z_{DET2})^2)^{.5}$

$v = l_{endet1}t_{odet2} / \text{deltat}$

$E1 = .5 * M * v^2$

$E_n = E1 / (\cos(\theta))^2$

$\text{minimum}E = \text{MIN}('E_n)$

$\text{maximum}E = \text{MAX}('E_n)$

$\text{Min}\theta = \text{MIN}(' \theta)$

$\text{Max}\theta = \text{MAX}(' \theta)$

$\text{minlength} = \text{MIN}(' l_{endet1}t_{odet2})$

maxlength=Max('lendet1todet2)

mintime = Min('deltat)

maxtime = Max('deltat)

totalE=Sum('En)

nbar=totalE/1000

ssqddata=(En-nbar)^2

ssqd=Sum('ssqddata)/(999)

\* Eavg1=En/1.602e-13

\* sigmas1=4.83/((Eavg1)^.5)-.578

\* Sigmas1=Nh\*sigmas1\*1e-24

\* Lambda1= 1/Sigmas1

\* Eavg=E1/1.602e-13

\* sigmas=4.83/((Eavg)^.5)-.578

\* Sigmas=Nh\*sigmas\*1e-24

\* Lambda= 1/Sigmas

\* thetaavg=Sum('theta)/1000

\* thetaspread=(theta-thetaavg)^2

\* thetavar=Sum('thetaspread)/999

== PROCEDURE FUNCTION: Xi ===== For Academic Use Only

Comment: Generates random numbers

Parameter Variables: random

Input Variables: seed1

Output Variables: xi

S Statement

---

MaxLong:= 2147483647

ModFactor:=7.826369259425646e-6

if seed1=0 then seed1=random

y=seed1\*MaxLong-.5

x=ModFactor \* ROUND(y)

seed2=x-INT(x)

if seed2 = 1 then xi=random

if seed2<1 then xi=seed2

== UNIT SHEET == For Academic Use Only

From	To	Multiply By	Add Offset	Comment
nanosec	sec	1E-9		
cm	m	.01		
MeV	joules	1.602E-13		
MeV <sup>2</sup>	joules <sup>2</sup>	2.566404E-26		
cm <sup>2</sup>	barn	1E24		

== GLOBAL SHEET == For Academic Use Only

Display Intermediate Values: Yes

Stop on List Error: No

Use Automatic Iteration:	Yes
Comparison Tolerance:	.000001
Typical Value:	1
Maximum Iteration Count:	20
Global Numeric Format:	
Append Variable Names:	Yes
Use Page Breaks: No	
Number Pages:	Yes
Form Length:	66
Printed Page Length:	60
Printed Page Width:	80
Left Margin:	0
Printer Device or Filename:	e:\msdat\error.asc+
Printer Setup String:	
Plot Output Filename:	TKPLOT.OUT
Use Color: Yes	
Slow Redisplay:	Yes
Solid Line Headings:	Yes
Bottom Prompt Line:	Yes

### Vita

Lieutenant Commander Wood was born on [REDACTED] Jackson, Mississippi. Shortly after graduation from Central High School in 1971, he joined the Navy and proceeded to serve in several combat roles in Southeast Asia. In 1975 he applied for and was accepted into the Navy Enlisted Scientific Education Program (NESEP), where he earned his Bachelor of Electrical Engineering degree from Auburn University. Upon graduation he was commissioned an Ensign in the United States Navy and served as the Assistant Weapons Officer on board the U. S. S. Lafayette (SSBN - 616 Blue) and as the Weapons Officer on board the U. S. S. Von Steuben (SSBN - 632 Blue) until 1985. Following his tours at sea he changed designators to become a Engineering Duty Officer, where he served at the Polaris Missile Facility Charleston, South Carolina. While serving in this billet, he was responsible for development of the Limited Life Component Exchange (LLCE) program for the Mark IV warhead. Upon activation of the program, he entered the School of Engineering, Air Force Institute of Technology, in August 1989.

Permanent Address: [REDACTED]  
[REDACTED]

### References

1. Allen, William D. *Neutron Detection*. New York: Philosophical Library Inc, 1960.
2. Ajzenberg-Selove, Fay. *Nuclear Spectroscopy*. New York: Academic Press Inc, 1960.
3. Kirk, F. W., "Neutron Time-Of-Flight Spectrometers," *Nuclear Instruments and Methods*, 162: 539-563 (1979).
4. Knoll, Glenn F. *Radiation Detection and Measurement*. New York: John Wiley & Sons, 1989.
5. Benedict, Manson And Pigford, Thomas H. And Levi, Hans W. *Nuclear Chemical Engineering*. New York: McGraw-Hill Book Company, 1981.
6. Cross, William G. And Ing, Harry. "Neutron Spectroscopy," *The Dosimetry of Ionizing Radiation*, Volume 2, edited by Kenneth R Kase. Orlando: Academic Press Inc, 1987.
7. LaMarsh, John R. *Introduction to Nuclear Reactor Theory*. Reading Massachusetts: Addison-Wesley Publishing Company, 1972.
8. Kumar, Arun and Nagarajan, P. "Neutron Spectra of  $^{239}\text{Pu}$ -Be Neutron Sources," *Nuclear Instruments and Methods*, 140: 175-179 (1977).

REPORT DOCUMENTATION PAGE

Form Approved  
 GSA GEN. REG. NO. 2704-0188

1. AGENCY USE ONLY (Leave blank) 2. REPORT DATE  
 March 1999 3. REPORT TYPE AND DATES COVERED  
 Master's Thesis

4. TITLE AND SUBTITLE  
 Construction, Calibration and Use of a Neutron Time-of-Flight Spectrometer 5. FUNDING NUMBERS

6. AUTHOR(S)  
 Charles L. Wood LCDR, USN

7. PERFORMING ORGANIZATION NAME(S) AND ADDRESS(ES)  
 Air Force Institute Of Technology  
 WPAFB OH 45433-6583 8. PERFORMING ORGANIZATION REPORT NUMBER  
 AFIT/GNE/ENP/9]M-]2

9. SPONSORING MONITORING AGENCY NAME(S) AND ADDRESS(ES) 10. SPONSORING MONITORING AGENCY REPORT NUMBER

11. SUPPLEMENTARY NOTES

12. DISTRIBUTION AVAILABILITY STATEMENT  
 Approved For Public Release; Distribution Unlimited 13. DISTRIBUTION STATEMENT CODE

14. ABSTRACT (Maximum 200 words)  
 The energy spectrum of a 5 curie Pu-Be neutron source is determined by use of a neutron time-of-flight spectrometer. This spectrometer measures the time it takes for a neutron to travel between two plastic scintillator detectors. Using a fixed distance for travel, a time spectrum is generated which is then unfolded into the energy spectrum of the source. The different aspects of equipment selection, connection and calibration of the system are described. With the resolved spectrum the energy resolution of the spectrometer is determined by using a Monte Carlo simulation of the experimental set-up. A dual-parameter experiment is conducted in which the proton recoil spectrum from the first detector is placed in coincidence with the time-of-flight data. Comparisons with the published spectrum from Arun Kumar and P. Nagarajan are made.

15. SUBJECT TERMS  
 Neutron Spectrometers, Time-of-Flight Spectrometers, Neutron energy spectrum, Pu-Be Neutron Source Energy spectrum, ← 16. NUMBER OF PAGES  
 102

17. SECURITY CLASSIFICATION OF REPORT  
 Unclassified 18. SECURITY CLASSIFICATION OF THIS PAGE  
 Unclassified 19. SECURITY CLASSIFICATION OF ABSTRACT  
 Unclassified 20. LIMITATION OF ABSTRACT  
 SAR